Title: *In vivo* microstimulation with cathodic and anodic asymmetric waveforms modulates spatiotemporal calcium dynamics in cortical neuropil and pyramidal neurons.

Authors: Stieger KC[1,2], Eles, JR[1], Ludwig, KA[3,4], Kozai TDY[1,2,5-7]

1. Department of Bioengineering, University of Pittsburgh, Pittsburgh, PA
2. Center for the Neural Basis of Cognition, University of Pittsburgh, Carnegie Mellon University, Pittsburgh, PA
3. Department of Biomedical Engineering, University of Wisconsin Madison, Madison, Wisconsin
4. Department of Neurological Surgery, University of Wisconsin Madison, Madison, Wisconsin
3. Center for Neuroscience, University of Pittsburgh, Pittsburgh, PA
4. McGowan Institute for Regenerative Medicine, University of Pittsburgh, Pittsburgh, PA
5. NeuroTech Center, University of Pittsburgh Brain Institute, Pittsburgh, PA

Abstract:
Electrical stimulation has been critical in the development of an understanding of brain function and disease. Despite its widespread use and obvious clinical potential, the mechanisms governing stimulation in the cortex remain largely unexplored in the context of pulse parameters. Modeling studies have suggested that modulation of stimulation pulse waveform may be able to control the probability of neuronal activation to selectively stimulate either cell bodies or passing fibers depending on the leading polarity. Thus, asymmetric waveforms (*i.e.* increasing the leading phase duration and proportionately decreasing the amplitude) may be able to activate a more spatially localized or distributed population of neurons if the leading phase is cathodic or anodic, respectively. Here, we use two photon and mesoscale calcium imaging of GCaMP6s expressed in excitatory pyramidal neurons of male mice to investigate the role of pulse polarity and waveform asymmetry on the spatiotemporal properties of direct neuronal activation with 10 Hz electrical stimulation. We demonstrate that increasing cathodic asymmetry effectively reduces neuronal activation and results in a more spatially localized subpopulation of activated neurons without sacrificing the density of activated neurons around the electrode. Conversely, increasing anodic asymmetry increases the spatial spread of activation and highly resembles spatiotemporal calcium activity induced by conventional symmetric cathodic stimulation. These results suggest that stimulation polarity and asymmetry can be used to modulate the spatiotemporal dynamics of neuronal activity thus increasing the effective parameter space of electrical stimulation to restore sensation and study circuit dynamics.

Significance Statement: Electrical stimulation has promise to restore sensation and motor function, as well as treat the symptoms of several neurological disorders. However, the mechanisms responsible for the beneficial effects of stimulation are not fully understood. This work supports modeling predictions by demonstrating that modulation of the stimulation waveform can dramatically affect the spatial recruitment and activity level of neurons *in vivo*. These findings suggest that stimulation waveform represents a parameter that may be able to increase the dynamic range of stimulation applications. Further characterization of these parameters with frequency, and amplitude could provide further insight into the mechanisms of electrical stimulation.

1. Introduction:

Implantable stimulating and recording microelectrodes have been fundamental to our understanding of the nervous system. The ability to perturb the brain with electrical stimulation has allowed us to realize localized functions of different brain areas[1] in addition to the functions of specific neural circuits[2, 3]. Additionally, there is strong evidence for the ability of intracortical microstimulation (ICMS) to provide sensory feedback in neural prosthetics and potentially restore sight to the blind [1, 4-23]. Although the use of electrical stimulation has provided critical knowledge to our understanding of the

brain, and can relieve symptoms of some neurological disorders[24-26], our poor understanding of the variability in neuronal recruitment to different stimulation parameters has prevented us from fully understanding the brain and how circuits change in disease[27].

Neuronal representation of sensory information is highly complex [28], and the ability to selectively recruit neuronal populations proximal to the electrode by varying pulse amplitude, frequency, or polarity, could provide the ability to represent neural activity matching physiological response patterns [29-41]. For example, neuronal adaptation is a common response to sustained stimuli and is believed to allow for the brain to better respond to transient stimuli [42]. Therefore, the ability to selectively modulate neuronal adaptation to electrical stimulation could help to produce more naturalistic and complex neuronal activity [31]. Furthermore, current stimulation parameters have poor selectivity, and neuronal recruitment depends on the complex order of cells dendrites and axons in the surrounding environment [43, 44]. Electrical stimulation often activates axon nodes, or terminals as opposed to cell bodies due to the higher excitability, thus the local axonal projections greatly influence the spatial distribution of activated neurons [33, 45-47]. Additionally, neuronal entrainment to stimulation depends on the site of activation on the neuron, the afterpotential dynamics, and the relative amount of excitatory and inhibitory input to the cells [38-40, 48, 49]. Our group recently published a study demonstrating that frequency can also modulate the spatial pattern of neuronal activation [41]. Specifically, distal neurons fail to entrain to frequencies ≥ 30 Hz, resulting in a dense population of neurons activated near the electrode. On the other hand, 10 Hz stimulation resulted in steady and spatially distributed neuronal activation. Therefore, consideration of the role of the neuronal element being activated (site of activation; *e.g.* soma, axon, dendrite), its afterpotential dynamics, and baseline excitability, in addition to the neuronal geometry around the electrode during stimulation, could help inform our ability to encode complex sensory information with ICMS.

Modeling [50-52] and *in vivo* [44-46, 53] studies have demonstrated that orthodromic activation of cells, and antidromic activation of passing fibers have similar thresholds when using monophasic stimulation pulses[38]. Therefore, it had been proposed that modulation of the likelihood of a neuronal element being activated by electric field may change the neuronal response to electrical stimulation [38, 39, 49]. Although monophasic waveforms have lower activation thresholds, convention is to use charge balanced biphasic waveforms for safety of the electrode; however, there can be safety benefits to slight charge imbalance [54-56]. Within these safety constraints, biphasic electrical stimulation pulse waveforms can be designed by altering the polarity of the leading or activation phase and/or the shape of each phase while maintaining an equivalent charge injection (so that the net injected charge is zero, or slightly reduced in the balance phase). Different waveform shapes have mainly been investigated to improve safety of stimulation; however, McIntyre and Grill [38, 39] investigated the effect of waveform asymmetry on the compartmental excitation of neurons. Specifically, they modeled the effect of increasing the duration and proportionately decreasing the amplitude of the leading phase of charge balanced waveforms on preferential activation of cell bodies or passing axons. The stimulation waveform was used to take advantage of the nonlinear dynamics of voltage gated sodium channels to modulate the probability of initiating an action potential due to stimulation from a given element. Their studies concluded that charge balanced asymmetric waveforms could selectively activate either cell bodies (cathodic first), or passing fibers (anodic first), depending on the leading polarity. Furthermore, proximal, or distal neurons had higher entrainment probabilities depending on leading polarity and frequency [38, 39]. These predictions were supported with an in vivo study by Wang and colleagues [57], however they only investigated the effect of a single pulse. By modulating the activity of the neurons using different stimulation waveform shapes during trains of stimulation, both neuronal entrainment and spatial recruitment could be selectively regulated, thus providing potential for more control over spatiotemporal dynamics of neuronal recruitment.

The present study aims to further characterize the role of stimulation waveform in neuronal activation to better understand the mechanisms underlying electrical stimulation using mesoscale, and

two photon calcium imaging. This study sought to answer two main questions, namely 1) Can stimulation waveform modulate the spatial distribution of neuronal activation? And 2) Do different populations of neurons prefer or entrain better to different stimulation waveforms? We address these questions in 4 sections using 30s stimulation trains delivered at 10 Hz to layer II/III of mice expressing the calcium sensor GCaMP6s in excitatory pyramidal neurons. In this way, we can observe the activation of the horizontal projections in layer II/III and decouple the spatial recruitment effects of stimulation waveform from the transient spatial activation of higher frequency stimulation [41]. In sections 3.1 and 3.2, we first address question 1 by quantifying the spread of activation defining an "activation area" metric under mesoscale imaging of a large spatial area (~2 mm) and two-photon microscopy imaging of neuropil activation, respectively. We then address question 2 by quantifying how the activation intensity changes over time and distance by measuring the fluorescence intensity dynamics (*e.g.* peak, mean, rate of change) on the two spatial scales, respectively. Next, we address both questions again in section 3.3, using two-photon microscopy to characterize direct neuronal activation by quantifying both the spatial properties of the activated neuronal population (*e.g.* density, mean distance) and the activation intensity over time. Finally, in section 3.4, we address question 2, by determining which cells were activated in common between different waveforms, and quantifying the relative activation level of a neuron to multiple waveforms. We demonstrate that stimulation waveform can be used to modulate the spatial selectivity as well as the strength of neuronal activation. The findings of this study ultimately support the claim that stimulation waveform can be an important tool in the modulation of neuronal activation, and highlights the importance of considering the nonlinear dynamics of ion channels when designing electrical stimulation protocols for better control of neuronal activation.

2. **Methods**

2.1 Animals and electrode implantation

Mature male, transgenic mice C57BL/6J-Tg(Thy1 GCaMP6s)GP4.3Dkim/J (>8 weeks, >28g, Jackson Laboratories, Bar Harbor, ME) were used in this study[58]. Subjects (n = 5-6 stimulation/implantation sites) were housed in 12h light/dark cycles with free access to food and water. Acute surgery and electrode implantation followed a protocol previously published [41, 59-68]. Mice were initially anesthetized with ketamine/xylazine (75mg/kg;7mg/kg) intraperitoneally (IP) and updated with ketamine (40 mg/kg) as needed (~ every hour). Mice were then placed on a heating pad and in a stereotaxic frame with continuous O_2 supply. After removing the scalp, a stainless-steel bone screw (ground and reference electrode) was placed over the motor cortex. The bone screw size and location were chosen to be sufficiently large and far away from the intended electrode implantation location (somatosensory cortex) so that the charge density was small, thus minimizing the interaction of the electric fields at the working and reference electrodes. This setup, therefore, is assumed to be monopolar and should limit any effect of bipolar pairs affecting the spatial pattern of neuronal activation. A dental drill was used to perform bilateral craniotomies (9-12mm^2) over the somatosensory cortices. Acute style 16-channel single shank Michigan style functional silicon probes with electrode site surface area of 703 µm^2 (A1x16-3mm-100-703; NeuroNexus, Ann Arbor, MI) were used for all stimulation experiments. Prior to implantation, iridium electrode sites were activated to increase charge storage capacity and 1kHz impedance was verified to be <500 kOhm[69]. Electrodes were implanted using an oil-hydraulic Microdrive (MO-81, Naishige, Japan) at a 30˚ angle into the somatosensory cortex to a final depth of 200-300 µm. To aid vascular visualization in two-photon experiments, sulforhodamine (SR101; 0.1 mg) was injected IP. Throughout the duration of the experiment, saline was used to keep the brain hydrated.

2.2 *Stimulation paradigms*

Stimulation was performed using a TDT IZ2 stimulator controlled by an RZ5D system (Tucker-Davis Technologies, Alachua, FL). Asymmetric pulses were designed such that any change in pulse width had a proportionate decrease in amplitude to maintain charge balance to the precision of the stimulator. An asymmetry index was defined similarly to Wang *et al.* 2012[57], as the ratio of the leading phase duration to the return phase duration minus 1 (1). For example, a symmetric biphasic pulse would have an asymmetry index of 0. All durations and amplitudes of the stimulation pulses are shown in Table 1.

The control stimulation is symmetric cathodic-first with 200 µs pulse width and 12.5 µA resulting in 2.5 nC/phase charge injection and 0.36 mC cm^{-2} charge density (703 μm^2 site area). This charge density is well within the Shannon limits, (k = [-0.06 -0.03]), however, because the site diameter is well below 200 µm (~15µm), the 4 nC/phase safety limit is more appropriate[70, 71]. Thus, these stimulation parameters are within suggested safety limits [16, 17, 55, 70-75]. Stimulation trials included a 30s baseline followed by a 30s stimulation duration and, either a 20s, or 60s post stimulation period for two photon, or mesoscale imaging respectively[41]. For each stimulation session, paradigms were applied in a random order.

$$Asymmetry\ Index = \frac{PW_l}{PW_r} - 1$$

Table 1: Stimulation parameters

2.5nC/phase, 0.36 mC/cm^2

Asymmetry Index	Leading Amplitude, µA	Leading Pulse Width, µs	Return Amplitude, µA	Return Pulse Width, µs	Total Pulse Time, µs
-1/2	± 12.5	200	∓ 6.2	400	1800
0	± 12.5	200	∓ 12.5	200	1200
4	± 2.5	1000	∓ 12.5	200	400
7	± 1.6	1600	∓ 12.5	200	600

In order to refer to specific stimulation parameters we use a letter to describe the polarity and a numbered subscript to describe the asymmetry index. For example, "C_0" refers to conventional symmetric cathodic leading stimulation. Similarly, "A_7" will be used to refer to anodic stimulation with an asymmetry index of 7.

2.3 Mesoscale and two photon imaging

To quantify neuronal activation outside the field of view (FOV) of two photon imaging, mesoscale imaging was performed during stimulation over a 3.7x3.0 mm window using an MVX-10 epifluorescence microscope (Olympus, Tokyo, Japan) and a CCD camera with a 50 ms exposure time (Retiga R1, QI imaging) at 20 Hz. A two-photon microscope (Bruker, Madison, WI) with an OPO laser (Insight DS+, Spectra Physics, Menlo Park, CA) tuned to 920 nm and kept below 40 mW was used for neuronal and neuropil imaging. The microscope was equipped with a 16X 0.8 NA water immersion objective (Nikon Instruments, Melville, NY) with a 3mm working distance resulting FOV of 407 x 407 μm^2 (512 x 512 pixels). Resonance mode was used to collect images at 30 Hz. Image acquisition was initiated by a trigger from the TDT system.

2.4 Image analysis and statistics

2.4.1 Stimulation inclusion

A total of 7 mice were used in this study to obtain a minimum of 5 stimulation trials for each condition[41], where 3 were used exclusively for two photon imaging, 3 were used exclusively for mesoscale imaging, and one mouse was used for both two photon and mesoscale imaging. A total of 6 stimulation sessions (1/hemisphere of one mouse) occurred for the 4 animals in the two-photon imaging, and 5 stimulation sessions occurred for the 4 animals in the mesoscale imaging. Separate stimulation trials were considered as different implant or electrode site locations. Cells and vasculature were used to verify minimal tissue displacement during each stimulation trial. Trials with observable tissue displacement were excluded from this study.

2.4.2 MVX GCaMP6s Quantification

All analysis of the MVX images was performed in Matlab (MathWorks, Boston, MA). The images were initially spatially smoothed using a gaussian filter with 2 standard deviations, then a 2x2 mm^2 ROI

was selected around the stimulation probe. Fluorescence was transformed into $\Delta F/F_0$ where F_0 is the mean fluorescence over the 30s pre-stimulus baseline. Each pixel was then filtered using a low-pass finite-impulse response filter (FIR) with a cutoff frequency of 2 Hz[76]. The asymmetric stimulation waveforms with a long leading phase used in this study are thought to modulate the spatial localization of neuronal activation through changes in activation threshold of target and off target sites of activation [38, 39]. Therefore, we aimed to evaluate the spatiotemporal dynamics of the effective spread of activation (activation area). Figure 1a shows the average neural recruitment over different 2s windows over the stimulation time. The pattern of activation spread radially and the intensity reduced with distance. Consequently, determine the spread of activation, the change in fluorescence was calculated in 20 µm radial bins radiating from the center of stimulation induced activation. A subset of these bins is overlaid on the activation images in Figure 1a, and the $\Delta F/F_0$ for these bins is plotted in Figure 1b. To calculate area of activation, an activation threshold was defined such that the average change in fluorescence in a bin needed to be 2 standard deviations above the mean continuously for 1 second (Fig. 1b). The area was then calculated for each frame as the area of the maximum activated bin, such that all smaller bins were also activated (Fig. 1c). This harsh thresholding aided in removing motion artifacts but did not alter the quantification of activation.

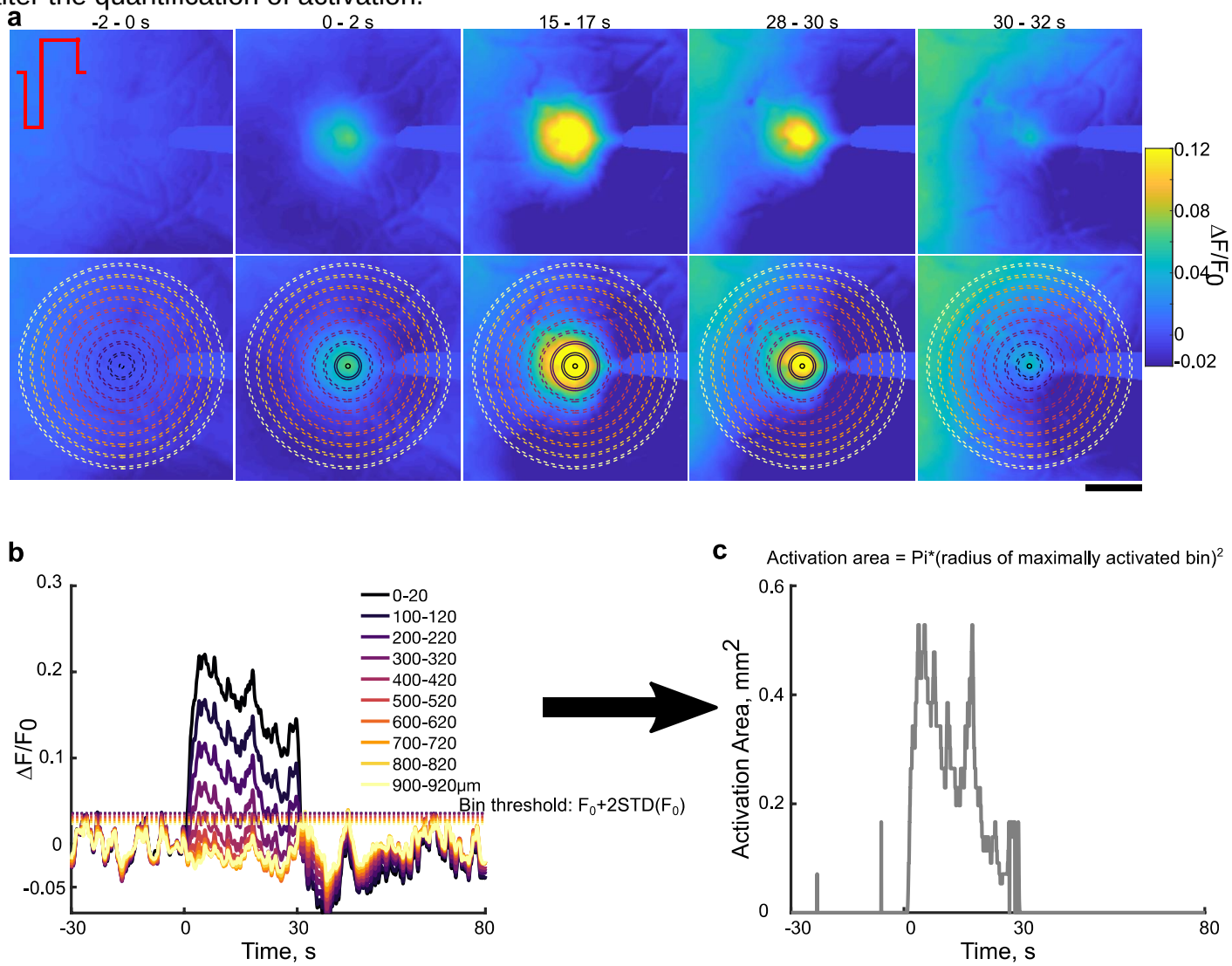

Figure 1. Quantification of activation area. (a) top: Representative $\Delta F/F_0$ images over the stimulation show that over time the spread of activation and intensity increases then decreases by the end of stimulation. Bottom: The same images in the top overlaid with a sub selection of radial bins used to calculate the fluorescence intensity and activation area. Solid lines represent activated bins. Scale bar is 500 µm. (b) The fluorescence intensity in the radial bins plotted in (a) with each bin's corresponding activation threshold (dotted lines). (c) Using the radius of the maximally activated bin with all smaller bins also activated, the activation area was calculated over time and shows an increase then a decrease over time.

Activation area generally tended to rise to a peak, then gradually decreased over the 30s stimulation, before stabilizing by the end of stimulation (Fig. 1c). Therefore, the peak, and the steady state area were calculated. Steady state area was defined as the average area during the last five seconds of stimulation because the area often plateaued during this time (Fig.1c). Specifically, how far from the electrode can neuronal elements be from the electrode, while still maintaining a significantly level of activation? Peak area can be interpreted as the maximum effective spread of activation for short duration stimulation trains (<5s), whereas steady state area would represent the maximum sustainable spread of activation for longer stimulation trains. Larger activation area could suggest greater antidromic activation of passing fibers, as opposed to orthodromic activation of neurons proximal to the electrode. Although the effects of electrical stimulation can be independent of synaptic transmission, it cannot be ruled out[33]. The time to peak area was quantified as a metric to describe the strength of activation at the stimulation onset. Additionally, because the activation area reduced over time, the percent change in area was calculated as the change in the mean area over the first and last 5 seconds of stimulation. One animal with a mean area of zero during the first 5 seconds for any stimulation paradigm were excluded from the analysis.

Next, because the stimulation waveforms are understood to modulate the activation thresholds of neurons, we aimed to evaluate the relative level of neuronal activity by quantifying the change in fluorescence over the 30 second stimulation. First, a distance threshold (0.98 mm) was defined as the minimum bin where the mean stimulation intensity of each stimulation condition was less than the grand mean plus one standard deviation of the mean (over 30s) at the maximum bin (1.4mm). Then the mean, peak, and slope of activation were calculated using the average fluorescence of this area for each stimulation condition. Peak and mean activation aim to represent how strongly neurons can entrain to the stimulation for short duration trains, and the relative level of sustained entrainment, respectively. Due to the kinetics of GCaMP6s, we are unable to accurately quantify the percent of 1:1 neuronal entrainment to the stimulation. However, because the fluorescence intensity increases with the number of action potentials in a short time[58], comparing the relative change in fluorescence can provide a rough approximation of the amount of entrainment. To calculate the slope of activation or inactivation, a first order polynomial was fit to the activation over the first or last two seconds of stimulation. Activation or inactivation slope represents the relative level of neuronal entrainment to a stimulation paradigm, where a greater magnitude slope implies greater activation. There was a substantial negative $\Delta F/F_0$ over a smaller area around the electrode that persisted for several seconds following the stimulation. To quantify this, the mean $\Delta F/F_0$ was calculated during the 10 seconds following stimulation over 0.4mm.

2.4.3 Neuronal soma quantification

For each stimulation session, neurons were manually identified using the 2D projection of the fluorescence standard deviation over the 30s stimulation and outlined using the ROI manager in ImageJ (NIH)[41]. The mean fluorescence intensity of each cell was extracted for further analysis in Matlab. The fluorescence intensity for each neuron was then processed similarly to the MVX images. Briefly, the mean intensity was transformed into $\Delta F/F_0$ and filtered using a low pass FIR filter with cutoff frequency of 2 Hz. In order to identify activated neurons, an activation threshold was defined as 3 standard deviations above the mean pre-stimulus fluorescence (F0). Neurons with suprathreshold fluorescence for at least 1 second over the 30 s stimulation were considered activated. To evaluate if stimulation polarity and asymmetry can be used to modulate the spatial localization of activated neurons, the spatial distribution of activated neurons around the electrode (*e.g.* distance and density) were analyzed. The distance of all activated cells was determined and placed in 20 µm radial bins to determine the spatial distribution and density of neurons activated by each stimulation condition. Quantification of how the intensity of fluorescence changes over the course of the 30s stimulation can provide insight into how well the neuron can entrain to a stimulus.

Our previous study demonstrated that stimulation induced neuronal activation falls into two broad groups: transiently activated neurons (onset) and neurons that remain activated for the duration of stimulation (steady state) [41]. To distinguish the timing of activation, cells were classified as “onset responsive”, “steady state responsive”, or “delayed responsive”. Neurons active during the first two seconds and not the last two where defined as onset. Neurons active during both the first two and last two were considered steady state. And neurons active during the last two seconds and not the first two were defined as delayed [41]. Here we implement a quantification previously used to examine the temporal characteristics of activated neurons, described as “activation time”. The activation time was calculated as the time for the fluorescence to reach half the peak cumulative fluorescence over the 30 seconds, that is, the time it takes to reach half the response energy[41]. The peak, mean, time to peak and slope of activation of neurons were determined similarly to the MVX activation.

Given the complex geometries of neurons around the electrode, it is possible that some neurons may entrain better to certain stimulation polarities and asymmetries. To quantify the differences in how the neurons were activated by each stimulation condition, we first determined which cells were activated in common between the different parameters. Next, an activation index ranging from -1 to 1 (Equation 2) was created to quantify how specific neurons respond to different stimulation conditions.

$$Activation\ index = \frac{X_1 - X_2}{X_1 + X_2} \quad (2),$$

Where X_1, and X_2 represent the two stimulation conditions being compared. For example, when comparing the mean activation, a value of zero would suggest comparable mean activation between the two stimulation conditions while deviation from zero would indicate stronger activation by one of the stimulation conditions (positive for X_1, negative for X_2). Statistical significance was determined by performing a Student’s t-test to determine if the activation index was significantly different from 0.

2.4.4 Neuropil Quantification.

To quantify changes in fluorescence of the neuropil which can have important calcium dynamics (axons, dendrites, out-of-plane neuronal somas), the electrode and all identified neuronal cell bodies were masked out (see section 3.4.3)[41, 77, 78]. Similar to section 3.4.2, the changes in neuropil fluorescence as $\Delta F/F_0$ were quantified in 20 µm radial bins radiating form the electrode site. Quantification of activation area (peak, steady state, mean, time to peak), and peak, mean, and activation/inactivation slope, of the fluorescence intensity were calculated as was done in section 3.4.2. Briefly, for activation area, bins were considered activated if their mean fluorescence intensity was above the mean plus 2 standard deviations above baseline fluorescence for one second consecutively. Area metrics represent the maximum and sustainable spread of activation for short or long duration trains, respectively. One animal was excluded from the time to peak area analysis because there was no area of activation for the C_4 condition. Fluorescence intensity quantifications were performed over all imaged bins to a distance of 260 µm from the electrode site. Activation metrics aimed to provide insight into the level of neuronal entrainment and activation modulation of the stimulation paradigms.

2.4.5 Statistical analysis.

All data in violin plots (Bastian Bechtold 2016, Violin plots for Matlab, https://github.com/bastibe/Violinplot-Matlab/blob/master/violinplot.m) show the mean (horizontal line), the median (diamonds), grey box plots, (25th and 75th percentiles, 1.5 times the interquartile range), scatter plot of the data within the kernel density estimate, with outliers as black “+”. In order to determine the interaction of asymmetry and polarity on outcome measures statistical analysis in violin plots was assessed with a two-way repeated measures ANOVA (2-way rmANOVA; alpha = 0.05), because the stimulation parameters in a trial were measured on the same neurons. This analysis was performed in R (R Core Team (2019). R: A language and environment for statistical computing. R Foundation for Statistical Computing,Vienna, Austria. URL https://www.R-project.org/.) using the ez package (Michael A. Lawrence (2016). ez: Easy

Analysis and Visualization of Factorial Experiments. R package version 4.4-0.https://CRAN.R-project.org/package=ez). Significance was assessed for neuron density and neuron number over distance (Fig. 6ab) using a three-way repeated measures ANOVA (polarity, asymmetry, distance). Lastly, students t-tests were used to determine activation indices significantly deviating from 0 (Fig. 8). Box plots show the mean (diamonds), the median (vertical line) and 25th and 75th percentiles, plus 1.5 times the interquartile range (whiskers). Outliers are represented with a black "+". In cases where sphericity was violated, the Greenhouse-Geisser method was used to correct degrees of freedom. Post-hoc analysis consisted of pairwise unequal variance (Welch's) t-tests with a Holm-Bonferroni correction. Data are described as mean ± standard deviation (STD).

3. Results

Our previous study using single shank Michigan-style electrodes implanted into the somatosensory cortex of mice expressing the calcium sensor GCaMP6s in pyramidal cells demonstrated that the spatial pattern of neuronal activation changed over time for frequencies above 10 Hz (see Fig. 5 Michelson *et al.* 2019) [41]. Because the aim of this study was to investigate if stimulation polarity and asymmetry can be used to selectively modulate the spatial and temporal patterns of neuronal activation with different waveforms, using the same model, we delivered 30s stimulation trains at 10 Hz, a frequency previously shown to have stable spatial activation over time. This allowed us to study the effect of stimulation waveform on the spatial pattern of activation, while decoupling the spatial fall off of neural activation at higher frequencies. All stimulation parameters delivered 2.48-2.56 nC/phase charge injection and 353-364 µC cm^{-2} charge density for 30s following a 30s baseline, and are compared to conventional symmetric cathodic first square wave with 200 µs pulse width and 12.5 µA amplitude similar to parameters used in human clinical ICMS applications (See Table 1)[2, 11, 17, 22, 41, 79, 80].

Evidence suggests that cathodic-first stimulation with positive asymmetric indices may modulate the relative amount of inactivated, or ready to be activated sodium channels of nearby neuronal elements to result in selective orthodromic activation. Conversely, anodic-first pulses may be more selective towards activation of passing fibers antidromically [14, 38-40]. We hypothesized that cathodic-first stimulation with a long activation phase would activate fewer passing fibers resulting in neuronal activation confined to a small area around the electrode. In contrast, anodic-first first pulses with large asymmetry index were hypothesized to activate passing fibers, thus resulting in more distributed neuronal activation at substantial distance from the electrode. Furthermore, it was predicted that different spatially distributed populations of neurons would have higher entrainment probabilities to different waveforms (proximal to cathodic, distal to anodic)[39]. In section 3.1 we show that stimulation waveform significantly influences the spread of neuronal activation as well as intensity of activation using mesoscale imaging by quantifying the activation area and magnitude of fluorescence change over time and distance (*e.g.* mean, peak, rate of change, time to peak). Because mesoscale imaging results in an average of the activation dynamics of multiple cortical layers, in section 3.2, we next perform the same analyses under two-photon microscopy to quantify the activation dynamics in the neuropil and show a similar trend. Next, in section 3.3 using two-photon microscopy we demonstrate that stimulation waveform can modulate the spatial localization of activated neurons without significantly sacrificing the density. Lastly because it was possible that stimulation waveform could be used to selectively activate either proximal or distal neurons (cathodic or anodic asymmetric respectively)[39] we quantify the similarity in the populations of neurons activated by the different waveforms and show that they are largely overlapping and are most strongly activated by cathodic stimulation with long return phase (*i.e.* second), and anodic stimulation with long activation phase (*i.e.* first).

3.1 *Mesoscale imaging reveals strong interaction of stimulation polarity and asymmetry on the spread of cortical pyramidal neuron activation.*

Figure 2 aims to address question 1 by determining the spatiotemporal spread of activation on a large spatial scale. The spread of activation increased radially with limited bias towards any specific direction (Fig. 2a). Therefore, in order to quantify the spread of activation, the change in florescence was measured in radial bins and the activation area was defined using the radius of the maximally activated bin ($\Delta F/F_0$> mean +2 STD), such that all smaller bins were also activated (Fig. 1). Interestingly, activation area often peaked within the first 10 seconds and gradually decreased over the duration of stimulation (Fig. 2b). As a measure of the spread of activation at the onset, we first quantified the peak area to represent the maximum spread of activation, where greater peak area could suggest greater antidromic activation for short duration stimulation trains (Fig. 2c). Previous work has shown that the direct response to electrical stimulation at threshold can be independent of synaptic transmission on small spatial scales [33]; however, monosynaptic connections can result in distal activation [79]. Thus, the distal activation on this spatial scale could involve synaptic propagation, especially on longer time scales. As asymmetry index was increased, peak activation area decreased for cathodic-first stimulation and increased for anodic first asymmetric pulses. Repeated measures two-way ANOVA revealed a significant interaction of polarity and asymmetry (n=5, p=0.0017). This is consistent with previous studies suggesting that pulse asymmetry modulates the probability of activating neurons antidromically, where a larger area would suggest greater antidromic activation [38, 57]. Quantification of the time to peak area was comparable across our parameters, suggesting that the spread rate of the initial activation may not be significantly influenced by pulse shape when delivered at 10 Hz (Fig. 2d).

Our previous two-photon study, demonstrated that activation of distal neurons (within 400µm) may be more stable at 10 Hz [41]; however, on a larger spatial scale, mesoscale imaging revealed a substantial decrease in activation area (within 1400 µm) over time that eventually stabilized during the last 10s of stimulation. Therefore, steady state area was defined as the average activation area during the last 5s of stimulation. This metric represents the spread of activation which can be sustained for longer stimulation trials, which are more common in deep brain stimulation. Steady state area followed the same pattern of activation as peak area, with asymmetric anodic-first stimulation having significantly greater area compared to symmetric anodic activation, and cathodic first asymmetric pulses (post-hoc Welch's T-test p<0.05; Fig. 2e). Despite the expectation that neuronal entrainment to 10 Hz stimulation would be high [41, 81], most stimulation asymmetries resulted in >50% reduction in the activation area between the first and last 5s of the train (Fig. 2f). Due to the averaging of calcium signal from multiple layers using mesoscale imaging, this reduction could be result from failed entrainment to antidromic activation [48, 49] or a reduction in synaptic propagation [79, 82] (see Discussion: 4.3). These data support the hypothesis that stimulation polarity and asymmetry may be able to selectively modulate the spatial spread of activation where cathodic first asymmetric pulses preferentially activate cell bodies. This may be important for stimulation of other brain areas or spinal cord where selective activation of passing fibers or the cell bodies could change which muscles become activated[39].

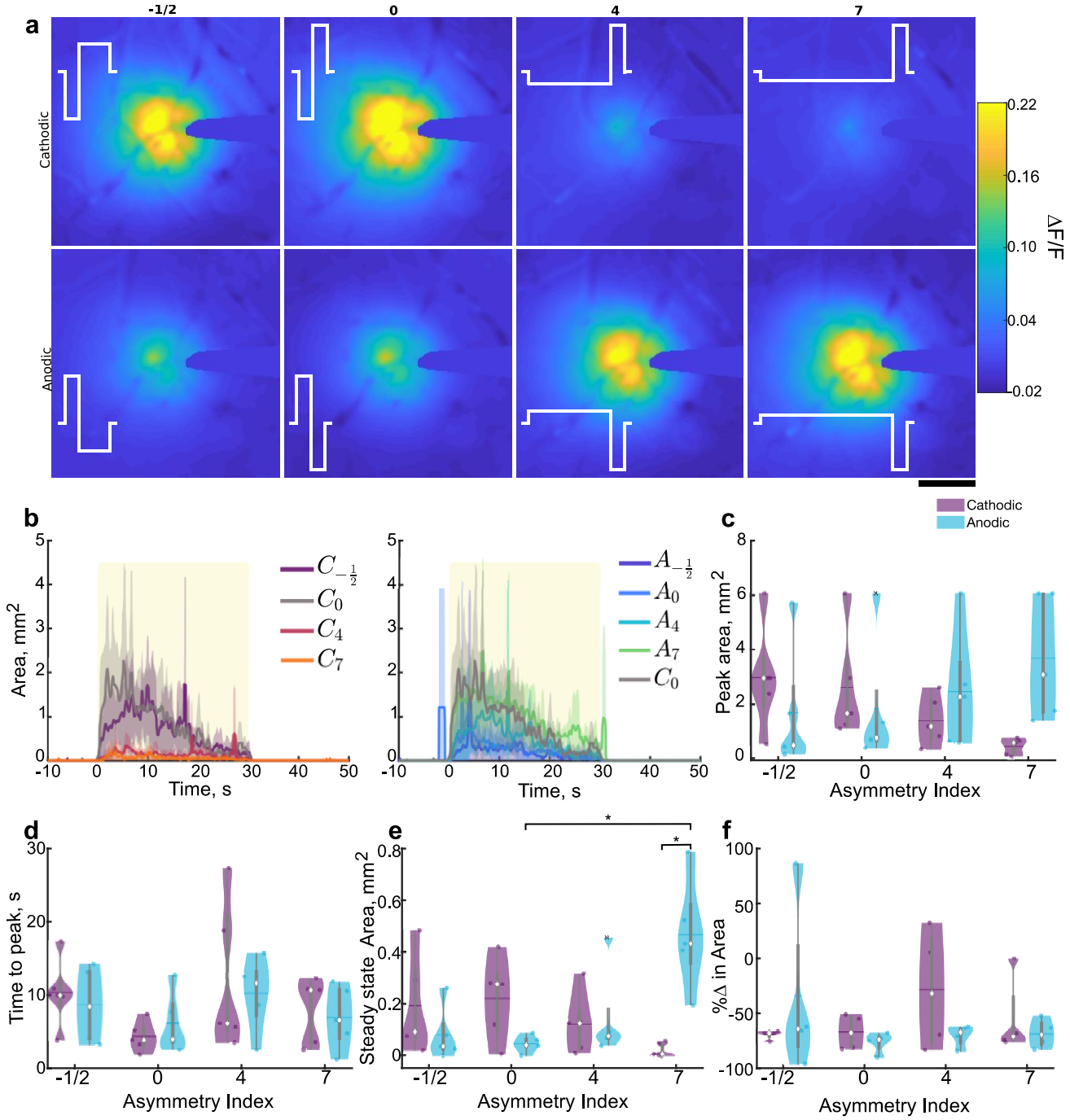

Figure 2: Stimulation polarity and asymmetry affect the spread of cortical activation during 30s stimulation trains under mesoscale imaging. (a) Representative mean $\Delta F/F_0$ over the 30s stimulation for the 8 different stimulation conditions. The stimulation waveform is represented in white, and the corresponding asymmetry index is displayed above. Scale bar indicates 500 µm. (b) Average (±SE; n=5) cortical activation area peaks early on (within 10-12s) and decreases over time and is comparable between $C_{-1/2}$, C_0, A_4, and A_7 and is reduced in C_4, C_7, $A_{-1/2}$, and A_0. Yellow box represents stimulation. (c-d) Peak (c; n=5, $F_{3,12}$= 9.54, p=0.0017) and time to peak (d) area during the stimulation train, where the median is indicated as a diamond and the mean indicated as a horizontal line in the violin plots. (e) Steady state area is increased in A_7 compared to A_0 and C_7 (n=5, $F_{3,12}$=10.36, p=0.0012). (f) Area rises and reduces over time resulting in a negative percent change in area for all stimulation conditions. Statistics were first assessed with a 2-way rmANOVA followed by post-hoc Welch's T-tests with Holm correction. * indicates p<0.05.

The magnitude of the mean fluorescence change was also modulated by stimulation waveform (Fig. 2a). We use this relative change in florescence as a rough approximation of neuronal entrainment to the different stimulation waveforms, although we are unable to differentiate 1:1 entrainment from bursting [58]. Thus, we next aimed to address question 2 by investigating the interaction of stimulation polarity and asymmetry on intensity of activation by quantifying the magnitude of fluorescence changes

over time and distance (Fig. 3). Similar to activation area, measuring the $\Delta F/F_0$ in radial bins revealed a transient activation that peaked early on and gradually reduced before plateauing by the end of stimulation (Fig. 3a). However, the $\Delta F/F_0$ appeared more stable for cathodic first asymmetric pulses with a long leading phase (Fig. 3a). Furthermore, averaging the $\Delta F/F_0$ over the 30s stimulation revealed an exponential decay with distance that became comparable by 980 µm from the electrode (Fig. 3b; see methods). Therefore, the $\Delta F/F_0$ was averaged over the first 980 µm from the electrode to compare across stimulation conditions. This averaging did not change the observed pattern of activation (Fig. 3c).

To evaluate how strongly neurons can entrain to stimulation, and how well that activation can be sustained, the peak and mean fluorescence was first quantified during the 30s stimulation train (Fig 2d-g). Similar to activation area, peak intensity can represent the relative neuronal entrainment during shorter stimulation trains, or potentially during temporally patterned stimulation. On the other hand, mean intensity would represent the neuronal entrainment during long stimulation trains, such as those used in deep brain stimulation. This quantification revealed a significant interaction between asymmetry and polarity for mean ($p<1e+5$) and peak ($p<0.001$) $\Delta F/F_0$. Increasing cathodic asymmetry resulted in a significantly reduced mean and peak $\Delta F/F_0$ compared to symmetric cathodic stimulation (Fig. 3 d-f). On the other hand, anodic-first pulses with the longest duration leading phase (A_7) resulted in an increased mean and peak activation intensity compared to symmetric anodic stimulation (Fig. 3 d-f). These results are consistent with the idea that, at the same charge injection, neuronal activation threshold is comparable for anodic first asymmetric pulses, and is increased for cathodic first asymmetric pulses [38]. Additionally, the reduced neuronal activation with cathodic-first stimulation with longer duration leading phases (C_4, C_7), and anodic first stimulation with a longer duration return phase ($A_{-1/2}$) could explain the increased behavioral detection thresholds previously observed for these stimulation parameters during shorter stimulation trains [35, 83]. It should be noted, however, that the geometry of fibers around the electrode and the choice of stimulation frequency can largely influence this entrainment [84].

The temporal dynamics of activation were quantified next. Our previous study demonstrated that the neuropil activation steadily increased over time for 10 Hz stimulation[41], therefore, it was possible that the $\Delta F/F_0$ would peak towards the end of stimulation. Fluorescence often peaked within the first few seconds of stimulation onset, however, for some asymmetric stimulation parameters, fluorescence continued to increase and peaked during the second half of the stimulation train (*i.e.* cathodic first with long activation phase, Fig. 3h). This suggested that neuronal entrainment could be changing over time. Therefore, the activation and inactivation slope were quantified by fitting a first order polynomial to the first or last two seconds of stimulation (Fig. 3 i-j). This “on slope” and “off slope” represent the initial and final levels of neuronal entrainment, respectively. There was a significant interaction of stimulation polarity and asymmetry for the activation slope ($F_{3,12}=9.16$, $n=5$, $p=0.002$), where Increasing asymmetry significantly reduced the activation slope for cathodic first pulses. The temporal differences observed here suggest that entrainment may be modulated over time. This may be important in the context of neural prosthetics where perceived stimulus intensity may depend on the number of action potentials. That is, pulse asymmetry could be used to encode stimulus intensity over time.

Lastly, several stimulation conditions were followed by a substantial and sustained reduction of fluorescence change, localized within ~400 µm around the electrode (Fig. 3ac). This was quantified by averaging the fluorescence change over the 10 s following stimulation (Fig. 3k). There was a significant interaction of stimulation asymmetry and polarity on the sustained reduction in $\Delta F/F_0$. This reduction decreased as cathodic asymmetry increased, but increased as anodic asymmetry increased. Reductions in neuronal activation have previously been observed after electrical stimulation[85]. It is unclear whether this reduction is neural fatigue, or inhibitory neurons influencing neuronal activity [86, 87].

Taken together, these results suggest that stimulation polarity and asymmetry can selectively modulate spatial localization of neuronal activation around the electrode. Specifically, increasing cathodic asymmetry increases the spatial localization compared to conventional symmetric stimulation, while increasing anodic asymmetry increases the similarity in activation with conventional symmetric cathodic stimulation. The reduced rate and magnitude of fluorescence change as cathodic asymmetry is increased, could suggest neuronal entrainment is being reduced, or that the fluorescence is restricted to the population of neurons around the electrode with limited antidromic activation of more superficial neurons. Specifically, the observed reduction in fluorescence change could be due to attenuation of the signal through the tissue, while the other stimulation parameters activate more Layer I neuronal elements, since mesoscale imaging averages over multiple cortical layers. To investigate this further, the same stimulation was performed under two-photon microscopy to visualize direct neuronal and neuropil activation around the electrode at higher spatial resolution.

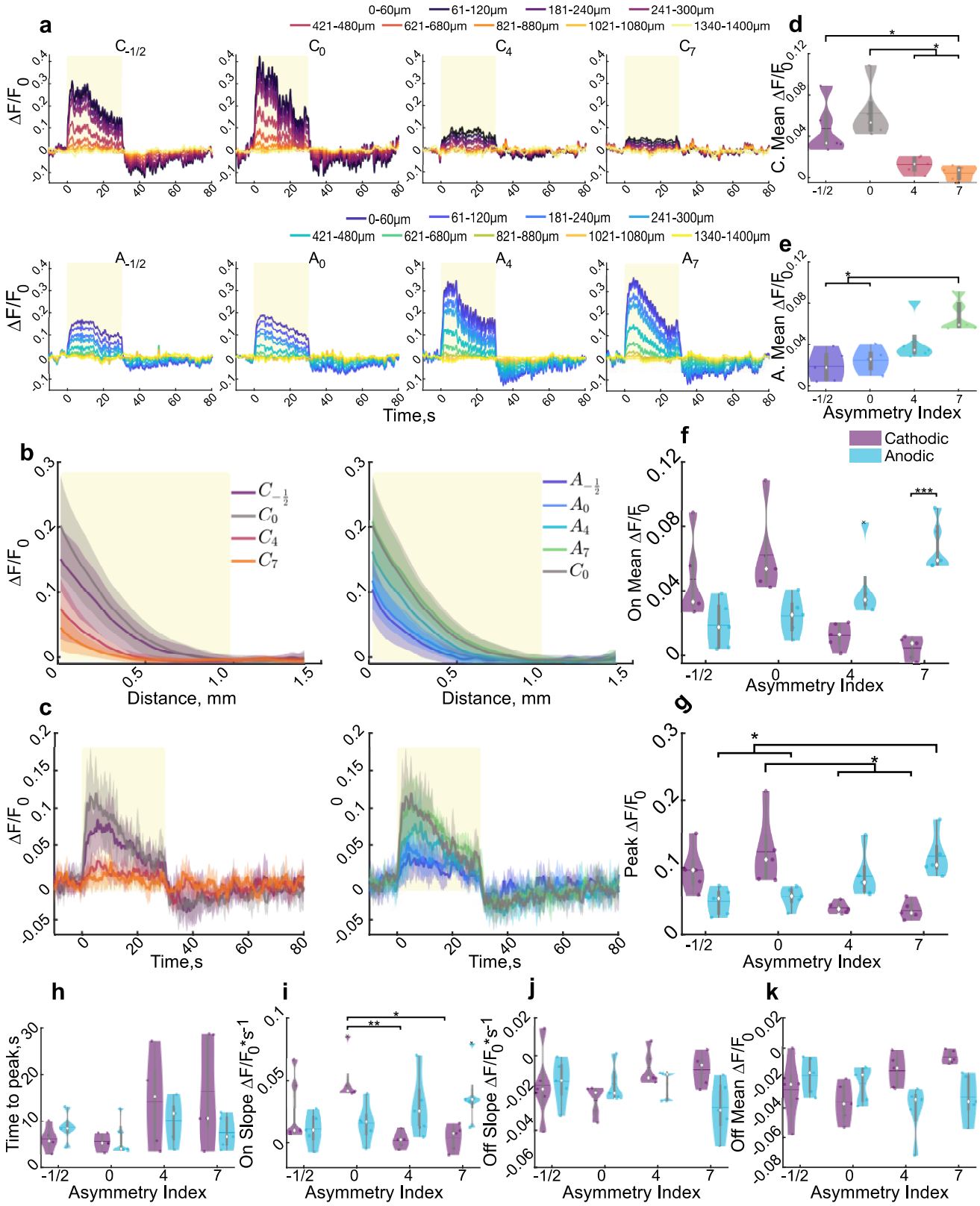

Figure 3: Stimulation pulse waveform and polarity modulate cortical neuronal activity under mesoscale imaging. (a). Cortical activity peaks within the first 15 seconds and reduces over time and distance for a representative animal then is inhibited for several seconds following stimulation. (b) the average (±STD) neuronal activity over the stimulation train reduces exponentially with distance from the electrode and is reduced in C_4 and C_7. Yellow rectangle indicates the distance (980µm) which will be averaged over for all but (k). (c) The average ± STD activation over 980µm follows the same pattern as the binned intensities. (d-f) Mean activation intensity over the stimulation period for the cathodic (d), anodic (e) and the interaction (f; $F_{3,12}$=30.87, n=5, p<1e-5). Cathodic and anodic were separated for clarity to show all post-hoc significance. (g) Peak activation intensity decreases or increases as cathodic or anodic asymmetry increases, respectively ($F_{3,12}$=14.36, p<0.001). (h) Time to peak activation over 980 µm during stimulation. (i-j) The activation (i; $F_{3,12}$=9.16, n=5, p=0.002) and inactivation (j) slopes of $\Delta F/F_0$ over 980µm. (k) The mean $\Delta F/F_0$ of the 10s post stimulation averaged over 400 µm shows

substantial reduction from baseline in all conditions (interaction $F_{3,12}$=8.38, n=5, p=0.0028). Statistics were first assessed with a 2-way rmANOVA followed by post-hoc Welch's T-tests with Bonfirroni-Holm correction. : * indicates p<0.05, ** indicates p<0.01, ** indicates p<0.001.

3.2 *Two-photon imaging demonstrates strong interaction of polarity and asymmetry on spread of neuropil activation*

Despite its superior spatial resolution, two photon microscopy images a single frame at a time. Therefore the investigation of neuronal activation may not be sufficient to comprehensively describe the effective spread of activation alone[23]. Consequently, we next aimed to address question 1 on a smaller spatial scale by quantifying the spatial localization of activation through neuropil fluorescence, as it contains axons, dendrites and out of focus neuronal somas, which may provide a better representation of the effective spread of cortical activation (Fig. 5)[23]. Figure 5a shows the standard deviation images of a stimulation session without neurons masked out to highlight how the neuropil activation relates to neuronal activation.

To quantify neuropil activation, neuronal somas were masked out, then the average $\Delta F/F_0$ in 20 µm radial bins radiating from the electrode site was calculated. Activation area of the neuropil was calculated similar to mesoscale imaging, as the area of the maximum activated bin given all smaller bins were also activated. While mesoscale imaging revealed a peak within the first 10 s (Fig. 3b), followed by a gradual decline, neuropil activation (within 260µm from the electrode site) was often more stable during stimulation, and followed a similar pattern for time to peak area as in Fig. 2d, with greater separation between waveforms with stronger and weaker activation (Fig. 4ab). Thus we are confident that on a small spatial scale with 10 Hz stimulation we can effectively investigate the effect of stimulation waveform on the spatial spread of activation while decoupling it from transient changes in the spatial spread of neuronal activity observed at higher frequencies [41]. Therefore, in addition to peak and steady state activation, the mean area was also quantified (Fig. 4c-e). There was a significant interaction of polarity and asymmetry ($F_{3,15}$=18.16, n=6, p<1e-4) on the steady state area, where increasing asymmetry for cathodic pulses reduced activation area, and increasing asymmetry for anodic pulses increased the area (Fig 3c). This effect was also present for mean (Fig. 4d; $F_{3,15}$ = 76.3, n=6, p<1e-8) and peak area (Fig. 4e; $F_{3,15}$=34.91, p<1e-6). These results further support the hypothesis that cathodic-first asymmetric pulses selectively activate fewer passing fibers resulting in a spatially localized area of activation. Similarly, increasing asymmetry for anodic stimulation pulses increases the area of activation suggesting greater activation of passing fibers. Furthermore, the time to peak area was elevated for cathodic stimulation with long activation phases (C_4, C_7) and anodic stimulation with symmetric phases or an increased return phase (A_0, $A_{-1/2}$) (Fig. 4f). Post-hoc analysis revealed an increased time to peak activation area for cathodic pulses with increased activation phase duration (C_4, C_7) compared to the other cathodic parameters (C_0, $C_{-1/2}$) suggesting that the activation of neurons could be increasing during the stimulation train.

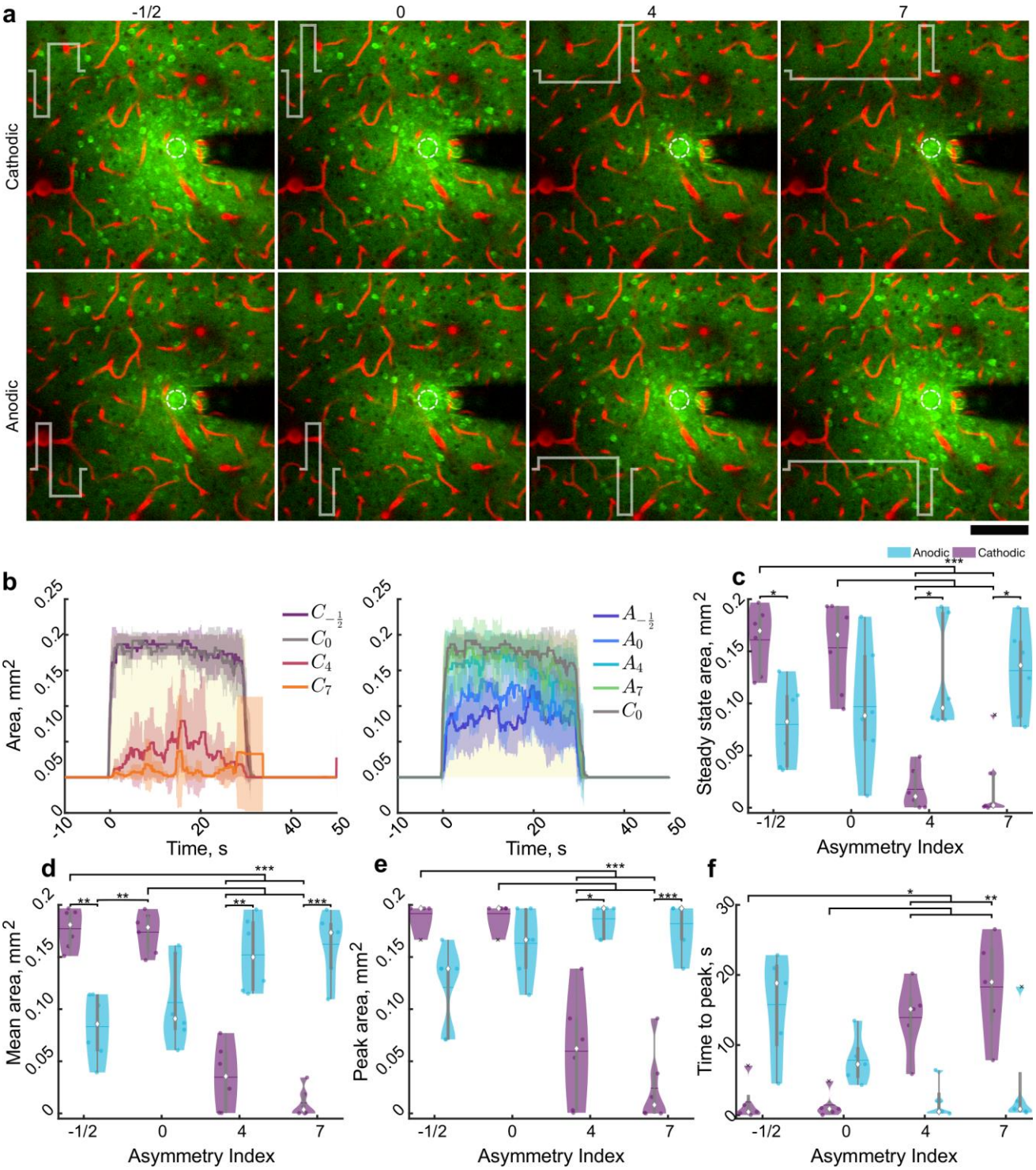

Figure 4: Stimulation polarity and asymmetry modulate the activation area of neuropil under two-photon imaging. (a) Representative standard deviation images over the stimulation train suggest stimulation waveform and asymmetry spread and intensity of neuropil (and neuronal activation). Stimulation waveform is represented in white, and the asymmetry index is displayed above the images. Scale bar represents 100 µm. (b) Average (±STD, n=6) neuropil activation area peaks early on after stimulation and is largely stable during stimulation and is reduced in C_4, C_7, $A_{-1/2}$ and A_0 compared to C_0, yellow box represents stimulation. (c-d) Stimulation polarity, asymmetry and the interaction significantly modulate the steady state (c; $F_{3,15}$=18.16, n=6, p<1e-4) average (d; F_{315}=76.31,n=6, p<1e-8), peak (e, $F_{3,15}$=34.9, n=6, p<1e-6), and time to peak (f, $F_{3,12}$=15.90, n=6, p<0.001) activation area over time. Statistics were first assessed with a 2-way rmANOVA followed by post-hoc Welch's T-tests with Holm correction. * indicates p<0.05, ** indicates p<0.01, *** indicates p<0.001.

Next, the spatiotemporal dynamics of the calcium transients in the neuropil were examined over the imaging plane in order to address question 2 on with finer spatial resolution and less laminal contamination (260µm) (Fig. 5). As with the activation area, the activation intensity remained relatively constant during stimulation while decaying exponentially with distance, although at a lesser degree than was observed under mesoscale imaging (Fig. 5ab, 2b). Consistent with mesoscale imaging, cathodic stimulation with either symmetric phases or increased return phase (C_0,$C_{-1/2}$) showed comparable neuropil entrainment with anodic first asymmetric stimulation with a longer activation phase (A_4, A_7), which were elevated compared to the other stimulation parameters (Fig. 5c). Quantification of the mean (Fig. 5d-f) , peak (Fig. 5g), and time to peak activation (Fig. 5h), as well as the rate of fluorescence change over the first and last two seconds of stimulation (activation/inactivation slope; Fig 4ij) revealed trends consistent with mesoscale imaging (Fig. 5d-j). Specifically, neuropil entrainment was reduced as asymmetry increased for cathodic stimulation and entrainment increased for anodic stimulation as quantified with the mean (interaction: $F_{0.96,4.88}$=48.6, n=6, p<1e-4), peak (interaction: $F_{0.93,4.64}$=45.06, n=6, p<0.001), activation ($F_{3,15}$=24.47, n=6, p<1e-5) and inactivation slope ($F_{0.7,3.52}$=21.25, n=6, p<0.0049), in addition to the time to peak fluorescence ($F_{3,15}$=5.06,n=6, p=0.013). These data could suggest that the cathodic asymmetric pulses may alter the activation threshold enough to activate only local neurons orthodromically; however, it could also suggest inconsistent activation due to a reduction in the entrainment probability.

Together, neuropil activation dynamics agree with the mesoscale analysis and suggest that the stimulation waveform likely plays a role in both the spatial spread of neuronal activation, as well as the entrainment. Specifically, cathodic asymmetric stimulation may activate only neurons in close proximity to the electrode, while anodic asymmetric stimulation may activate a pattern of neurons highly comparable to cathodic symmetric stimulation. Therefore, the spatial distribution of direct neuronal activation was subsequently evaluated.

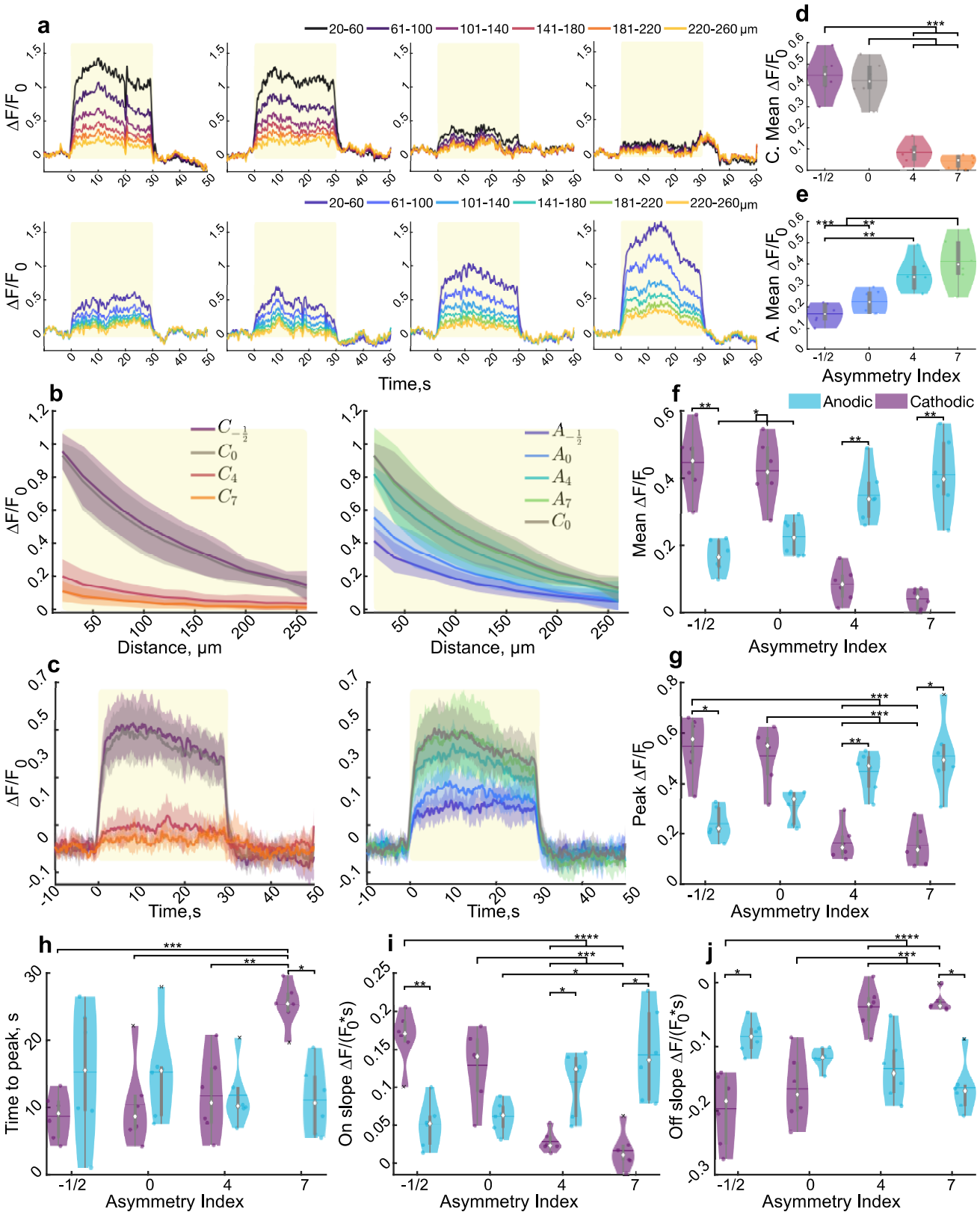

Figure 5: Stimulation polarity and waveform modulate the level of neuropil activation over time. (a) Representative $\Delta F/F_0$ in increasing radial bins during stimulation demonstrate differential effects of neuropil activation intensity with polarity and asymmetry. Yellow box represents stimulation. (b) The average stimulation over time (± STD) decreases exponentially over distance and appears reduced in C_4, C_7, $A_{-1/2}$, A_0 compared to C_0. Yellow box represents area to be averaged over for comparisons. (c) The average neuropil activation intensity (±STD) over 260µm rises rapidly then slowly increases followed by a slow decrease over time. (d-f) The average stimulation intensity of the neuropil in the imaging plane over the stimulation train is significantly reduced in C_4 and C_7 Compared to $C_{-1/2}$ and C_0, and is reduced in $A_{-1/2}$, and A_0 compared to A_7 ($F_{0.97,4.88}$=48.60, n=6, p<1e-4). (g-j) Peak (g, $F_{0.93,4.64}$=45.06, n=6, p<0.001), time to peak (h, $F_{3,15}$=5.06, n=6,

p=0.0128), activation (I; $F_{3,15}$=24.47, n=6, p<1e-5) and inactivation slope (j; $F_{0.70,3.52}$=21.15, n=6, p=0.0049) during stimulation averages over 260 µm. Statistics were first assessed with a 2-way rmANOVA followed by post-hoc Welch's T-tests with Holm correction : ** indicates p<0.01, *** indicates p<0.001.

3.3 Two-photon imaging of direct neuronal activation reveals consistent interaction of polarity and asymmetry on spatial recruitment and neuronal activity

After quantifying how stimulation waveform modulates the spatial activation on a large spatial scale and within the neuropil, we next aimed to address question 1 by characterizing the direct neuronal activation over distance. The spatial distribution of neuronal activation was quantified in order to determine if increasing cathodic asymmetry could increase the probability of selectively activating neurons orthodromically, where spatial localization, or distribution, would imply orthodromic or antidromic activation, respectively (Fig. 6.). After determining which neurons had fluorescence intensities 3 standard deviations above the mean for at least one second over the 30s train, the neuron's distance from the electrode was used to calculate the activation density. Neuronal density was calculated as the number of neurons within the binned area of circles with increasing radii by 20 µm. The density of neuronal activation around the electrode decreased exponentially with distance, and was significantly elevated in the first 40 µm compared to the area beyond 80 µm for all stimulation conditions, except the most asymmetric cathodic stimulation, which was not significantly different in any bin (Fig. 6a). Additionally, the number of neurons activated beyond the median distance of all activated neurons was significantly reduced for cathodic-first asymmetric stimulation with a long activation phase, whereas the number of neurons was not significantly reduced within the first 106 µm for slightly asymmetric cathodic stimulation (C_4; Fig. 6b). Furthermore, the mean distance of activated neurons was significantly modulated by stimulation polarity and asymmetry (Fig. 6c; interaction: $F_{3,15}$=27.84, n=6, p<1e-5). Specifically, the mean distance of activated neurons reduced as cathodic asymmetry increased and generally increased as anodic asymmetry increased. This interaction was also observed for the total number of neurons activated ($F_{0.78,3.89}$=17.60, n=6, p=0.0053; Fig. 6d). Consistent with both the mesoscale imaging and the neuropil quantification, these data suggest that stimulation polarity and asymmetry can be used to selectively activate different spatial populations of neurons. Specifically, asymmetric cathodic stimulation with a moderately increased activation phase (C_4) can selectively activate a spatially localized population of neurons, without sacrificing the density of activated neurons in close proximity to the electrode (see Section 5.4). Additionally, anodic first asymmetric stimulation with an increased leading phase duration activates a more distributed population of neurons, comparable to conventional symmetric cathodic stimulation.

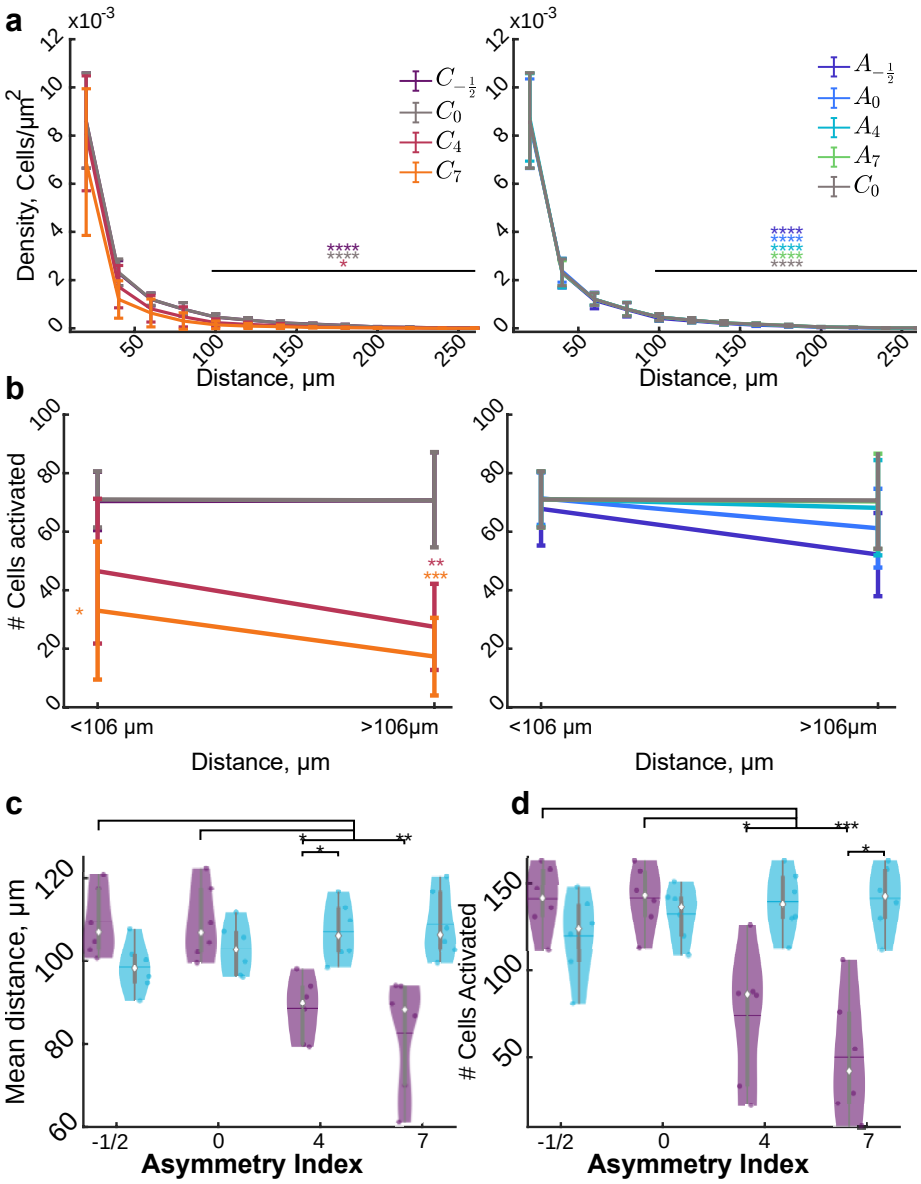

Figure 6: Stimulation asymmetry and polarity modulate the spatial distribution of neuronal activation. (a) The density of activated neurons within the first 40 µm of the electrode is significantly greater than the density of neurons beyond 40 µm in all conditions except C_7 ($F_{5,36}$ = 3.77, n=6, p<1e-10). (b) The number of activated cells is activated in relatively even amounts within all conditions except C_4 and C_7 where the majority of activated neurons ~70% is within the first 106µm. Data represented as mean ± STD ($F_{5,3}$=4.02, n=6, p<0.012). (c-d) Stimulation polarity and waveform modulate the mean distance of the activated neurons ($F_{3,15}$=27.84, n=6, p<1e-5) as well as the number ($F_{0.78,3.89}$=17.60, n=6, p<0.0053). Statistics were first assessed with a 3-way rmANOVA (a,b) or a 2-way rmANOVA (c,d) followed by post-hoc Welch's T-tests with Bonfirroni-Holm correction * indicates p<0.05, ** indicates p<0.01, *** p<0.0001, **** p<1e-5.

Next, the intensity level of neuronal activation was quantified to address question 2 and determine how the relative neuronal activation differed for these stimulation parameters in the neuronal populations as a whole (Fig. 7). It is important to characterize how neurons sustain activity to different stimulation parameters so that we can better understand how to improve implementation of stimulation in sensory prosthetics or in therapeutic applications like spinal cord stimulation. For example, understanding how neurons may adapt to a stimulation parameter could be useful in somatosensory restoration as adaptation to tactile information is common[42]. Therefore, the intensity changes and timing of activation were quantified.

There was a dynamic range of neuronal responses to stimulation (Fig 6a-b). In general, quantification of direct neuronal activation was consistent with the mesoscale imaging and the neuropil analysis, but with larger effect size. There was a highly significant interaction of polarity and asymmetry on

the mean, activation and inactivation slope, peak and time to peak fluorescence (all $p<0.001$). Specifically, neurons did not entrain as well to cathodic first asymmetric stimulation with increased activation phase duration, but gradually increased fluorescence (Fig. 7c-g). On the other hand, neurons activated by anodic first asymmetric stimulation with a long activation phase had highly comparable activation patterns with conventional symmetric cathodic stimulation. These results are consistent with the modeling by McIntyre and Grill, suggesting that the activation threshold for cathodic asymmetric stimulation would be higher than symmetric, and anodic-first stimulation would be comparable [38].

Our previous study classified the activation response of neurons into two general categories, onset, or steady state. Figure 7b shows that onset cells are transiently activated within the first two seconds and then fail to entrain to stimulation, while steady state cells, which were the majority, activate initially and continue to fire in response to stimulation (Fig. 7hi). In this study, there was a relatively rare third class of activation response, where the neuron does not become “activated” until a few seconds after the stimulation onset (Fig. 7b). These cells were defined as “delayed response” cells. There was a significant interaction of polarity and asymmetry on the percentage of delayed response cells ($F_{1.29, 6.47}=5.33$, $n=6$, $p<0.028$) and they were primarily only present in asymmetric cathodic first stimulation with a long activation phase (Fig. 7j). Finally, the activation time was quantified as defined by Michelson et al, as the time for the cumulative sum of $\Delta F/F_0$ to reach 50 % of the total sum[41]. In this definition, a neuron whose activity peaks and is maintained from 0-30s, will have an activation time of 15 s. Deviation in either direction from 15 seconds provides an idea of how well the neuron entrains to a given stimulation condition. For example, and onset neuron will often have an activation time of less than 15s, while a delayed cell will often have an activation time of greater than 15s. There was a significant interaction of stimulation polarity and asymmetry on the activation time, where increasing cathodic asymmetry resulted in a greater activation time (Fig. 7k). Because of the greater proportion of delayed response cells and increased activation time in cathodic first asymmetric stimulation with a long leading phase, it is possible that more cells around the electrode could be recruited during longer stimulation trials. That is, the benefit of spatial selectivity of this stimulation may be better suited for stimulation applications requiring long trains of stimulation. However, future studies should investigate the response types at more clinically relevant stimulation frequencies (*e.g.* 100 Hz) (see Section 5.1).

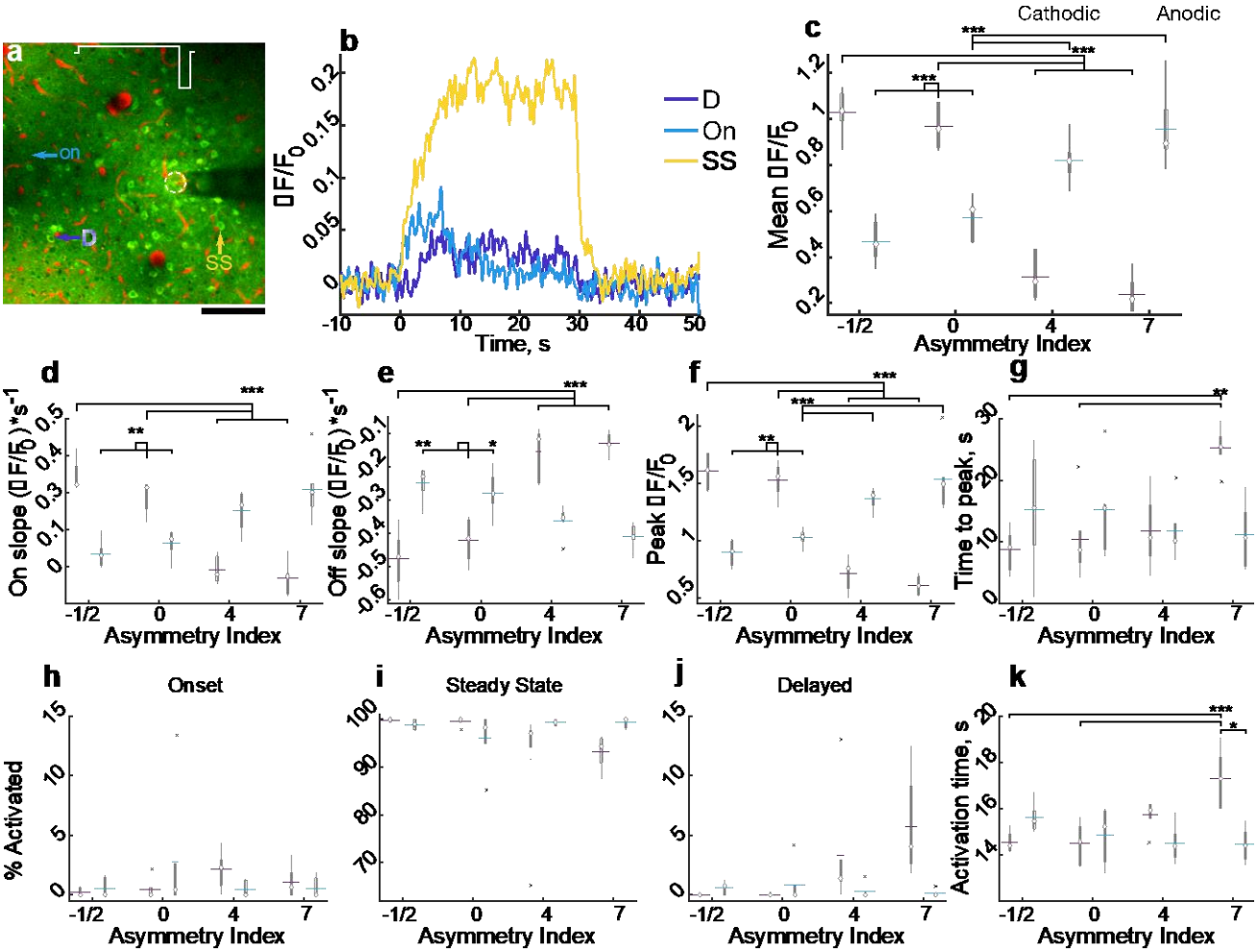

Figure 7: Stimulation asymmetry and polarity modulate neuronal activity. (a) Representative standard deviation image of neurons activated by A_7. (b) Representative traces of cells indicated in (a) for onset (On), steady state (SS), and delayed (D). Yellow rectangle indicates stimulation. (c-g) Mean (c, $F_{3,15}$=61.86, n=6, p<1e-7), activation(d; $F_{3,15}$=42.91, n=6, p<1e-6) and inactivation (e; $F_{0.72,3.61}$=44.62,n = 6, p<0.001) peak (e; $F_{0.95,4.74}$=56.40, n=6, p<1e-4) and time to peak activation (g; $F_{3,15}$=11.10, n=6, p<0.001) of cells averaged for each animal. (h-j) Mean percent of cells activated in each animal characterized as onset (h), steady state (I, $F_{3,15}$=3.52, n=6, p=0.041), or delayed (j; $F_{1.29,6.47}$=5.33, n=6, p=0.028). (k) Average weighted activation time of activated cells for each animal ($F_{3,15}$=10.04, n=6, p<0.001). Statistics were first assessed with a 2-way rmANOVA followed by post-hoc Welch's T-tests with Holm correction : * indicates p<0.05, ** indicates p<0.01, ** indicates p<0.001.

3.4 Stimulation polarity and asymmetry modulate population of activated neurons

The studies by McIntyre and Grill demonstrated that conventional symmetric biphasic cathodic first stimulation pulses activate local cell bodies and fibers of passage, while modulation of the waveform could selectively activate either, the cell local cell bodies (cathodic asymmetric with a long leading phase), or fibers of passage of distal but not proximal neurons (anodic asymmetric with a long leading phase) [38, 39]. This level of selectivity could be beneficial in cases such as the spinal cord where the fibers of passage that innervate some muscles can lie in close proximity to neuronal soma that innervate other muscles [39]. Therefore, the overlap in the neuronal populations activated by the different waveforms and their activation properties were measured in order to answer question 2 and quantify the selectivity and preference different populations of cortical neurons around the electrode (Fig. 8).

Figure 8a shows representative composite images of the activation patterns of neurons activated by conventional symmetric cathodic stimulation (green), overlapped with the activation pattern of neurons activated by the other polarities and asymmetries (red). Neurons and neuropil in yellow therefore

represent comparable activation levels. Although, there are some cells uniquely activated by the different stimulation conditions (white arrows) the populations were largely overlapping. However, of the neurons that were activated in common between all conditions, some neurons clearly preferred, or entrained better to, some stimulation waveforms to others (Fig. 8bc). To characterize the level of overlap, the percentage of neurons activated in common between two stimulation conditions was quantified and is shown as a heatmap in Figure 8d. For example, of the neurons activated by a stimulation condition on the y axis, what percentage of those neurons were also activated by the stimulation conditions on the x axis? This shows that while asymmetric cathodic stimulation activates a smaller subset of the neuronal population of neurons activated by the other conditions, the remaining conditions activated nearly all of the same neurons (>80%). This suggests that, in the cortex, while asymmetric cathodic first pulses with a long activation phase can activate a smaller subset of neurons around the electrode (Fig. 8d, Fig. 6), asymmetric anodic stimulation pulses with a long leading phase result in activation of both the neurons in close proximity to the electrode and distal neurons whose fibers of passage pass by the electrode.

Given that the different neuronal populations around the electrode (proximal vs distal) were predicted to entrain better to the different stimulation waveforms (cathodic asymmetric vs anodic asymmetric) [39], we next aimed to characterize the preference of activation to the different waveforms. This preference could therefore translate to greater perceived intensity of a localized or distributed stimulus. In general, of the neuronal population that was activated by all stimulation waveforms, the neurons entrained the most to anodic asymmetric stimulation with the longest leading phase (A_7) and cathodic stimulation with a longer duration return phase ($C_{-1/2}$; Fig. 8e-f). In order to quantify the preference between the different waveforms we defined an activation index ranging from -1 to 1, that directly compared the activation of a neuron to two different stimulation (See section 3.4.3). Any significant deviation from an activation index of 0 would represent preference for one of the stimulation waveforms being compared in each neuron. For example, when comparing the mean $\Delta F/F_0$ for conventional symmetric stimulation (C_0) with that of asymmetric cathodic stimulation with the longest activation phase (C_7), an asymmetry index greater than 0 would show preference for conventional symmetric cathodic stimulation, while an asymmetry index less than 0 would show preference for asymmetric cathodic stimulation. Figure 8g shows the activation indices of waveform comparisons for neurons in the cathodic (top), anodic and symmetric cathodic (middle), and neurons activated by all conditions compared to symmetric cathodic stimulation (bottom). Significance was assessed with single sample student's t-tests. These results are consistent with previous figures, where, on average for each animal, neurons preferred cathodic stimulation that was symmetric (C_0) or had longer duration return phase ($C_{-1/2}$), and asymmetric anodic stimulation (A_4, A_7) to other waveforms. Additionally, neurons responded similarly across the preferred waveforms, with the exception that neurons preferred cathodic stimulation with an increased return phase compared to conventional symmetric cathodic stimulation. Interestingly, the activation time between conditions was generally more comparable in all groups except among cathodic stimulation parameters (Fig. 8h).

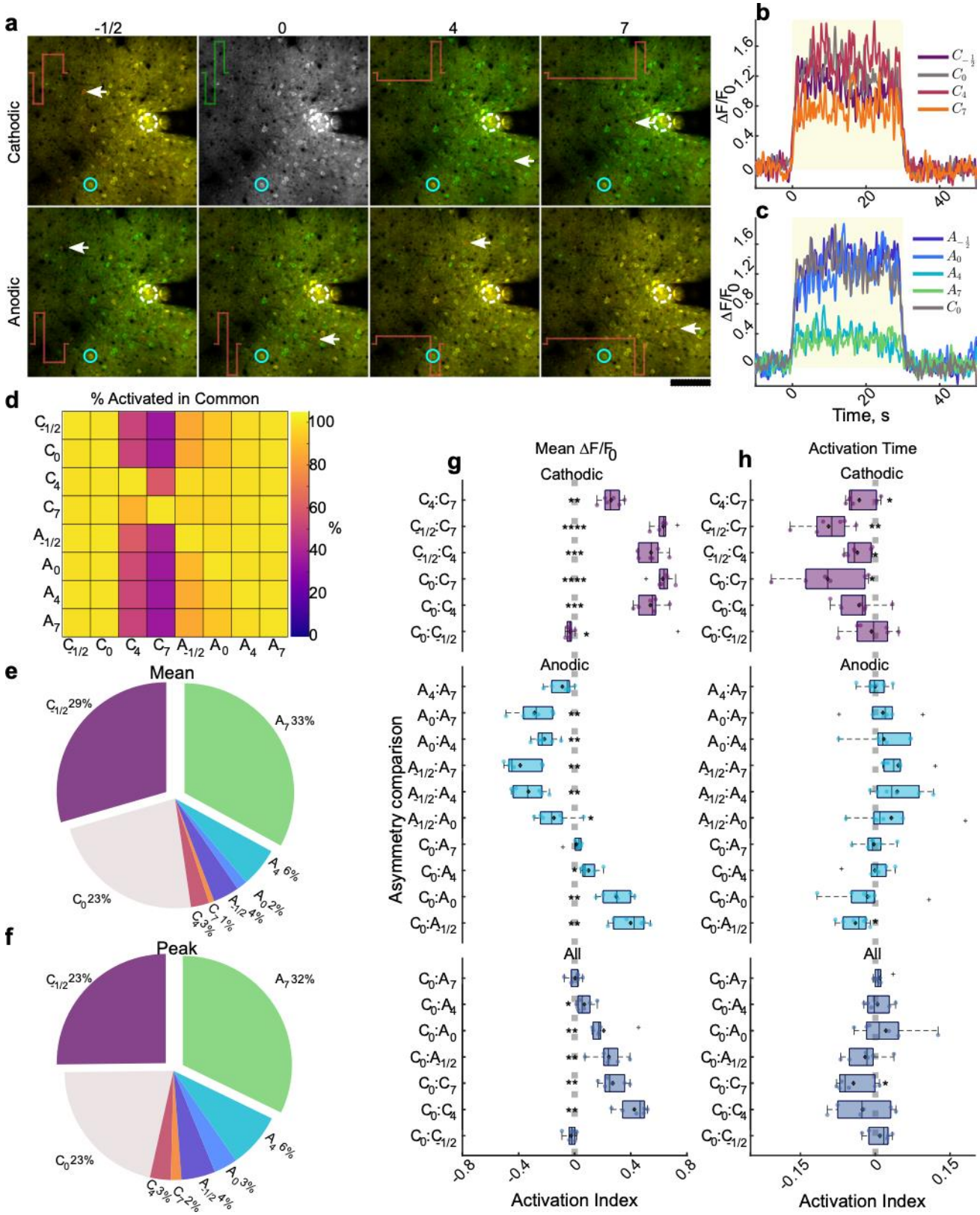

Figure 8: Population of activated cells is largely overlapping between stimulation conditions, and the level of activation is comparable between C_0, $C_{-1/2}$, and A_7. (a) Representative composite standard deviation images of the cells activated by conventional C_0 in green, or each respective stimulation waveform in red. Yellow cells represent neurons activated by both stimulation conditions. Note the relative level of overlap between $C_{-1/2}$, C_0, A_4, and A_7. White arrows signify cells activated by comparison waveform that was not activated by symmetric cathodic stimulation. (b-c) Representative traces of neuron indicated by blue circle in (a) activated by each stimulation waveform. (d) Heatmap of the cells activated in common between the conditions on the vertical and horizontal axis. The values represent the percent of cells activated by the vertical condition that were also activated by the condition on the horizontal axis. Note the nearly 100 % overlap of activation for all conditions except C_4 and C_7. (e-f) Pie charts of the relative percent of neurons in the population activated by all

conditions that preferred (greatest mean (e) or peak(f) each stimulation condition. (g-h) Activation index of the relative mean (g) or activation time (h) for each comparison where the activation index ranges from -1 to 1 and a positive index indicates greater magnitude of the first condition in the comparisons. N=6 for each t-test. * p<0.05, ** p<0.01, *** p<1e-5, ****p<1e-8.

Table 2: Waveform effects on spatial selectivity and neuronal activation

	Asymmetry Waveform		Spatial localization	Activation probability
Cathodic	$C_{-1/2}$		↓↓	↑↑↑
	C_0		↓↓	↑↑↑
	C_4		↑↑	↓↓
	C_7		↑↑	↓↓↓
Anodic	$A_{-1/2}$		↓	↓
	A_0		↓	↓
	A_4		↓↓	↑↑
	A_7		↓↓	↑↑↑

Table 2: Waveform effects on spatial selectivity and neuronal activation. Increasing cathodic asymmetry increases spatial localization and reduces neuronal activation. Increasing anodic asymmetry reduces spatial localization and increases neuronal activation. Arrows represent the level of spatial localization or neuronal activation where ↑↑↑ represents the greatest amount and ↓↓↓ represents the least amount.

4. Discussion

Given that performance of stimulation can be highly variable, it is critical to identify how stimulation parameters affect the tissue surrounding the electrode. In particular, the spatial distribution, relative spike rate, and number of activated neurons [13, 43, 88-91]. Here, we investigated the role of stimulation pulse polarity and asymmetry delivered at 10 Hz in a monopolar configuration on these properties on two different spatial scales. Specifically, we consider how increasing, or decreasing, the duration of the activation phase relative to the return phase of the stimulation (positive vs negative asymmetry index, respectively) pulses for both cathodic-first and anodic-first stimulation affects the spatiotemporal activation of neurons around the electrode. Although 10 Hz stimulation is substantially lower than what is used clinically [11], it allowed us to decouple the spatial effects of stimulation waveform from the high frequency mediated inactivation of distal neurons (within 400 µm)[41]. We used both mesoscale and two photon imaging to better quantify the spatial scale of neuronal activation with different stimulation waveforms. The results are summarized in Table 2 and demonstrate that modulation of the stimulation waveform strongly affects both the spatial localization of neuronal activation, and the relative entrainment of neurons to a 30s stimulation train delivered at 10 Hz. Specifically, increasing the duration and proportionately decreasing the amplitude of the leading phase of biphasic cathodic first stimulation pulses increases the spatial localization of neuronal activation, and reduces entrainment. Conversely, the same manipulation for anodic leading stimulation increased both the entrainment probability and the spatial spread of activated neurons. However, on a large spatial scale (2x2 mm), all stimulation conditions resulted in a reduction in spatial spread of neuronal activation over time possibly suggesting a possible reduced activation for distal neurons outside of the two-photon imaging frame (~1400 µm).

Finally, while these results show that stimulation waveform can modulate the spatial localization of neuronal activation, the population of neurons activated by different asymmetric waveforms was largely overlapping, with neurons preferring symmetric cathodic stimulation and asymmetric anodic leading stimulation with the longest leading phase. Together these results demonstrate the value of stimulation waveform as a tool to modulate the spatial localization of neuronal activation as well as the effective entrainment of neurons to the stimulus.

4.1 *Biophysics of stimulation pulse asymmetry*

Electrical stimulation aims to activate neurons by redistributing ions in the complex tissue geometry around the electrode such that the extracellular environment close to neuronal voltage sensitive sodium channels can become sufficiently negative to depolarize the membrane potential and increase the probability of firing an action potential [92]. In fact, monophasic waveforms can increase the selectivity of neuronal element activation (*i.e.* soma, axon) at lower thresholds than biphasic waveforms [38, 44, 93]. Additionally, shorter pulse durations require exponentially higher amplitudes for effective neuronal activation [39, 45, 47, 93]. This property is often used to characterize the excitability of a neuron to a stimulation pulse [45, 47], where the minimum current amplitude required to elicit an action potential with a long pulse width is called the rheobase current, and the pulse duration required to elicit an action potential at twice the rheobase current is the chronaxie time [45, 52]. However, despite being less effective at activating neurons, biphasic, charge balanced waveforms are often used to limit tissue damage and electrode corrosion [38, 54, 55, 92]. Different stimulation waveforms have been investigated to reduce activation thresholds by making the biphasic waveform appear more monophasic to the tissue [34, 54]. For example, a short interphase period between the injection and balance phase can be introduced, and the amplitude of the return phase can be reduced. These waveforms effectively allow the electric field to persist in the tissue longer and increase the probability of activation [34, 37, 54]. We use stimulation waveforms with an asymmetry index of -1/2 (long return phase) to investigate these effects on direct neuronal activation around the electrode. The position of the electrode relative to the different neuronal elements also affects the site of activation on the neuron [49]. Therefore, modulation of the pulse waveform in terms of relative phase duration and polarity, as investigated here, are likely to differentially affect the electric field in the complex extracellular environment and change the pattern of neuronal activation. It is important to note; however, although stimulation waveforms may be charge balanced, it is possible that they are not electrochemically balanced, which can be harmful to both the electrode and the tissue [54]. A long duration activation phase may allow more electrochemical species to dissipate too far from the electrode preventing the charge from being recovered during the return phase, thus resulting in irreversible Faradaic reactions. This may be especially present in trains of pulses, and can be more probable for anodic first pulses. In fact, even increasing the duration of the return phase can reduce the safety for the tissue[54]. We did not observe any gas bubble formation (indicative of the potential exceeding the water window) in any of our experiments; however, other irreversible reactions could have occurred[54]. Future work should evaluate the safety of these waveforms for both electrode and tissue damage.

In this study, we investigate how modulating the ratio of the leading phase pulse width to the balancing phase pulse width modulates the activation of cortical pyramidal neurons around the electrode. For both cathodic an anodic leading polarity, the asymmetries range from doubling the duration of the return phase relative to the activating phase, to increasing the duration of the activation phase by a factor of 8 relative to the balancing phase (See Table 1). In order to maintain charge balance, any increase in phase duration was matched with a proportionate decrease in amplitude. This essentially results in a long duration subthreshold leading phase that takes advantage of the nonlinear conductance properties of different neuronal elements or compartments to modulate their activation probabilities, where the second phase is considered the activation phase [38, 39]. Because the site of activation can change with electrode location, these asymmetric waveforms can slightly depolarize off target ele-

ments, while hyperpolarizing target elements. The long duration subthreshold depolarization of off target elements aims to increase the number of inactivated sodium channels, while the hyperpolarization of target elements aims to increase the open probability of the inactivation gate, therefore priming them for activation. Additionally, these effects depend on the second spatial derivative of the electric field as a function of the pulse amplitude [44, 52], where in the complex environment would result in different areas of inactivation and activation on neurons and fibers around the electrode. It is possible this could significantly affect the activation and entrainment probability. The modeling predicts that asymmetric cathodic first stimulation pulses with a long duration subthreshold activation phase will selectively activate cell bodies around the electrode, asymmetric anodic first stimulation pulses with a long duration activation phase can selectively activate passing fibers, and finally, symmetric biphasic (cathodic or anodic first) can activate both cell bodies and passing fibers. Because the activation threshold of cortical neurons exponentially decreases with pulse width [45], (strength duration relationship) it is possible that shorter asymmetric pulse durations could have more differential effects. We investigate multiple asymmetry indices in order to determine an effective range of pulse durations to improve selectivity of activation. These waveforms, therefore, are hypothesized to modulate the spatial selectivity of neuronal activation (proximal, distributed, or distal) and relative levels of neuronal activation.

*4.2 Stimulation polarity and asymmetry selectively modulate the **spatial** dynamics of neuronal activation*

Electrical stimulation-mediated spatial activation pattern of neurons surrounding an electrode is complex and believed to be a largely influenced by the axons passing by the electrode as well as their baseline excitability and branching geometries within the network of neurons and non-neuronal cells [14, 23, 33, 44-46, 52, 85, 94-96]. Here, we show that ICMS of layer II/III of the mouse somatosensory cortex with biphasic stimulation pulses of varying shapes and polarity result in strong neuronal or neuropil activation around the electrode that reduces exponentially with distance from the electrode (Fig. 2,3,5). The electric field around the electrode decreases with distance likely resulting in fewer activated neuronal elements and thus fewer neurons are activated at large distances from the electrode [23]. Additionally, the electrode location with respect to different neuronal elements, and the stimulation polarity and waveform all can affect the site of activation on the neuron (soma, axon initial segment, node of Ranvier) which can impact the spatial distribution of neuronal activation [38, 49, 93]. These results are consistent with the prediction that symmetric stimulation pulses will activate both neuronal axons and cell bodies, resulting in neuronal activation in close proximity and at distal locations from the electrode [38, 39].

The effect of stimulation asymmetry on activation of different neuronal elements has been investigated before in both neuromeric and psychometric analyses [35, 57, 83] supporting the modelling predictions [38, 39]. Specifically, Wang and colleagues showed that microstimulation of a rat thalamic barreloid with a single pulse of cathodic leading asymmetric stimulation with a long leading phase resulted in a smaller and targeted area of cortical activation, while anodic leading asymmetric stimulation resulted in a larger more directionally shifted area of cortex compared to symmetric cathodic stimulation and mechanical whisker stimulation [57]. They concluded that the leading polarity of the stimulation determined how many passing fibers projecting to different cortical barrels were activated. However, when they used similar pulse parameters to directly stimulate layer 4 of the rat barrel cortex, they did not observe a difference in spatial localization of neuronal activation between symmetric and asymmetric cathodic leading stimulation [83]. This is in contrast to our finding that increasing the asymmetry of cathodic first stimulation pulses significantly reduced the spread of cortical activation. These contrasting results can likely be explained by the difference in the neuronal projection anatomy in layer 4 where Bari and colleagues stimulated, versus layer II/III of the cortex, where our electrode was placed. While the axonal projections to the superficial layers of cortex is largely restricted to a single cortical column, layer II/III has greater horizontal projections that can span more than one column [83, 97]. The horizontal projections of layer II/III thus allowed us to effectively determine how stimulation waveform can

modulate the spatial localization of neuronal activation, and therefore, the selectivity of activating cell bodies or passing fibers. Additionally, the previous studies measured cortical activity with voltage sensitive dye imaging, which can represent subthreshold and suprathreshold neuronal activation. Our study built on these by using calcium imaging and longer stimulation trains to observe both neuronal and neuropil activation over time.

We show that cathodic leading asymmetric waveforms with long activation phases significantly reduce the spread of both neuronal and neuropil activation, which suggests that these waveforms can effectively reduce the activation of passing fibers of distal neurons. However, while increasing the asymmetry of anodic first stimulation pulses can increase the spatial spread of neuronal activation, neurons proximal to the electrode are also activated. This is in contrast to modeling that predicted neurons near the electrode had significantly poorer entrainment to asymmetric anodic stimulation compared to cathodic symmetric and asymmetric stimulation [39]. A possible explanation is that the fibers of these proximal neurons are therefore being activated by the stimulation, resulting in antidromic somatic activation proximal to the electrode. It is possible; however, that these effects are a product of the asymmetric pulses with a long activation approximating monophasic stimulation, where anodic leading asymmetric stimulation would resemble cathodic monophasic pulses, and cathodic leading stimulation would resemble anodic monophasic pulses. This can explain the similarity in both the spatial distribution and activation intensity observed between symmetric anodic stimulation (A_0) with cathodic asymmetric stimulation with a long activation phase (C_4, C_7), and similarly for cathodic symmetric, and anodic asymmetric. Further experiments would need to be done in order to determine the site of activation, but in practice, we show that 10 Hz cathodic first asymmetric stimulation activates a spatially localized population of neurons, while anodic first asymmetric stimulation activates a distributed population of neurons similarly to conventional symmetric cathodic first stimulation. While anodic first asymmetric stimulation with a long leading phase did not limit the activation to somas distal from the electrode, it is possible that the distal neurons whose axons pass by the electrode could entrain better to these pulses versus conventional symmetric cathodic stimulation [39]. We chose 10 Hz stimulation to limit the effect of inactivation distal neurons observed during higher frequency stimulation [41, 81], but future research should investigate higher and more clinically relevant stimulation frequencies to further characterize the neurometric differences of these waveforms. Overall, this suggests that cathodic first asymmetric stimulation could be an effective tool to for localized artificial percepts in neural prosthetics, or even to limit undesired off target activation in spinal cord stimulation.

*4.3 Stimulation polarity and asymmetry modulate the **spatiotemporal** dynamics of neuronal activation*

Somatic entrainment to electrical stimulation depends on the site of activation, which is largely determined by the location of the electrode relative to the neuron [38, 40, 44, 48, 49]. Specifically, neuronal elements have different afterpotential dynamics and excitability levels, which can affect the preferred frequency of activation [39, 48]. Specifically, because the axon initial segment has a high concentration of potassium channels, neuronal soma can entrain much more strongly to high frequency stimulation than stimulation at more distal nodes [48]. It is important to note, however, that the axon may be able to entrain with higher fidelity than the soma at high frequencies of stimulation [49]. In fact, using optogenetics, it was shown that pyramidal neurons have difficulty entraining to stimulation frequency above 15 Hz [81]. Consistent with our previous study [41], we show relatively stable neuronal activation to 10 Hz stimulation under two photon imaging; however, under mesoscale imaging, we observe a substantial decrease in the spread of activation over time. Because we did not use synaptic blockers (*e.g.* CNQX, APV) it is unclear how much the reduction in distal activation is from neurons directly or indirectly (transapically) activated [82]. Mechanisms governing poor entrainment of distal neuronal somas are likely to involve lateral inhibition [49, 87], ion buildup [48, 98-100], fatigue[86], virtual anode formation [41, 44, 92, 95], or even geometrical branching of axons [47, 101]. We showed that the density

of neuronal activation decreased exponentially with distance, therefore it is likely that there is less potassium build up at those distal locations, therefore decreasing the activation and entrainment probability of those soma [48, 99, 100, 102]. However, the involvement of inhibitory neurons in lateral inhibition and nonneuronal cells should not be ignored, as they are crucial components of information processing in neuronal circuits and can regulate neuronal activation due to electrical stimulation [85, 87, 103-106]. Inhibitory synaptic input into neurons can greatly reduce the entrainment probability of neuronal somas, especially without excitatory input (ketamine anesthesia blocks NMDA receptors) [49]. Furthermore, lateral inhibition plays a critical role in containing the horizontal spread of neuronal activation in the cortex [87]. Although this reduction in somatic entrainment distal to the electrode is more prevalent at higher frequency [41], the fact that is observed even at lower frequencies and the presence of the effect is independent of stimulation waveform merits further investigation into the roles of other cell types and especially lateral inhibition in electrical stimulation.

To further support this claim, mesoscale imaging allowed visualization of the neural population activated across layers and revealed a prolonged substantial reduction in fluorescence intensity following stimulation. While a reduction in neuronal activity following stimulation has been observed before, it is not entirely clear if inhibition or other cell types may play a role [85, 87]. The reduction in neuronal activity was substantially stronger for stimulation conditions that resulted in the largest increase in activation during the stimulation. It is possible then, that this increased activity also resulted in increased inhibitory recruitment therefore reducing the activity at the end of the train since inhibition is critical in the pattern of neuronal activation to electrical stimulation [87]. Future research utilizing fluorescent GABA sensors could aid in better understanding the role of inhibition[107]. However, because this effect was not observed during two photon imaging it is possible that the reduction in activity could be a reduction in the entrainment of distal neurons within a column. Specifically, mesoscale imaging averages the neuronal activity of several layers, and a reduction in layer I neuronal activity without a reduction in layer II/III activity could still result in a decreased activation area. Layer I activity could be from either antidromic activation or from synaptic connections. Furthermore, since astrocytes are key regulators of neurotransmitter clearance, and astrocytic voltage changes can influence the efficiency of this regulation [85] they are likely to influence the entrainment of somas. Because this reduction in activity can even occur for short stimulation, it should also be investigated in the context of temporal patterning of stimulation, which has shown promise for deep brain stimulation [108]. Ultimately, multimodal imaging allowed further insight into the spatial dynamics of neural activation and the role waveform plays in shaping recruitment of different neurons.

It is important to consider how this activation may translate to ICMS in human patients where the distance between layers is larger and the electrode location within a layer may vary during implantation. Using 1.5 mm Utah arrays, implanted into the human somatosensory cortex, it is possible that some electrodes are within layer II/III and therefore the results here should be comparable [11, 109-111]. Importantly, we show that distal or superficial neurons, whether activated antidromically, or through synaptic activation, reduce their level of activation over time. This could suggest that the activation of neurons whose axons pass by the electrode in layer II/III could fail to be activated at longer duration stimulation trains, especially as the neuron-electrode distance increases, such as deeper cortical neurons in the human as this distance is greater than that in the mouse [110, 112]. This effect may also be particularly prominent as the frequency of stimulation increases [41]. Therefore, careful consideration of the electrode placement within the cortex could help explain variability in the effects of stimulating different electrodes or decreased perceptual intensity over time [22, 25].

4.4 *Stimulation polarity and asymmetry modulate neuronal* ***activation***

Electrical stimulation pulse width, frequency, and waveform modulate the psychometric outcomes if ICMS [11, 17, 18, 35, 83], therefore it is important to understand how these parameters modulate the direct neuronal activation. Multiple studies showed that the behavioral detection threshold for cathodic first asymmetric stimulation is increased compared to symmetric cathodic stimulation [11, 61], which

therefore could be due to fewer neurons being activated, or lower firing rates of the neurons during the stimulation. Cell body activation with cathodic first asymmetric stimulation is likely to have a larger activation threshold, which would result in fewer neurons becoming activated and potentially poorer entrainment to stimulation trains [38]. Here we show that as asymmetry increases for cathodic first stimulation, both the relative firing rates of the neurons activated (mesoscale, neuropil and direct neuronal activation), and the number of neurons activated are reduced. Furthermore, the rate of fluorescence rise at the onset of stimulation is also significantly reduced compared to symmetric cathodic stimulation. While the neuronal activation with these waveforms could increase over time, it is possible that the reduction in the number of neurons activated and the onset entrainment of these neurons explains the increased behavior detection thresholds observed previously [35, 83]. Alternatively, because we show that these cathodic first asymmetric waveforms activate a more localized area of cortex, it is also possible that the artificial sensation produced is also more localized than that produced with symmetric stimulation. Because this difference may produce a different perceptual quality, the animals may not judge the perception the same. However, it is important to note that the neuronal entrainment to these waveforms may increase with increased frequency based on the afterpotential times of the neuronal components being activated or inactivated [39]. Therefore, to achieve better entrainment and lower detection thresholds with more localized activation, higher stimulation frequencies in addition to higher amplitudes may be beneficial when using asymmetric cathodic stimulation.

Increasing asymmetry of anodic first stimulation, on the other hand, increased the neuronal entrainment probability at the onset, and throughout the duration of stimulation. Previous psychometric comparison of these waveforms showed that asymmetric anodic stimulation had highly similar detection thresholds compared to symmetric cathodic stimulation [35]. Our results qualify this by showing that the entrainment, and rate of rise and decay of the fluorescence, is highly comparable between cathodic symmetric and anodic asymmetric stimulation. In fact, we show that the excitatory neuronal population activated by these different waveforms is nearly identical. Therefore, it is likely that at 10 Hz asymmetric anodic first stimulation results in highly similar activation patterns as cathodic symmetric stimulation. However, because anodic asymmetric stimulation may be activating different neuronal elements, and this can result in differential entrainment properties of the soma and axon, it will be important to better understand how the entrainment changes at frequencies where somatic entrainment is reduced[39, 41, 49].

We also show that increasing the duration of the return phase relative to the activation phase of cathodic stimulation activates neurons similarly or even to a higher level to symmetric stimulation, while this waveform modulation results in a minor reduction in neuronal activation for anodic first stimulation. For cathodic stimulation, this type of asymmetric waveform is often more effective at activating neurons because it allows the tissue to react to the charge for a longer period of time [34]. Therefore, they can often have lower detection thresholds[35, 37]. While anodic stimulation can be more effective with certain neuronal and electrode geometries[29], ICMS is often less effective with anodic pulses [17, 33, 35]. This could be because the first phase of anodic stimulation can hyperpolarize some elements, resulting in the second phase being the activation phase. This is generally referred to as anodal break stimulation [92, 95].

Our results show strong similarities between anodic stimulation with short activation phases, and cathodic stimulation with long activation phases, as well as between cathodic stimulation with short activation phases and anodic stimulation with long activation phases. This may be because as the duration of the activation phase increases (with a proportionate amplitude reduction) the waveform approaches monophasic stimulation, where neurons are activated during the second phase. Consequently, stimulation waveforms where the effective activation phase is anodic ($A_{-1/2}$, A_0, C_4, C_7) would result in similar activation patterns, and similarly for cathodic activation phases ($C_{-1/2}$, C_0, A_4, A_7). The reduction in activation we observe for pulses with an anodic effective activation phase could be a result of the increased activation threshold for anodic pulses[38], and would explain the higher behavioral

detection thresholds [35, 83]. It would be expected that decreasing amplitude for cathodic leading pulses would result in similar levels of activation and spatial recruitment. However it is possible that utilizing the asymmetric pulses could provide a better dynamic range of stimulation amplitude (intensity of activation) with limited change in the spread of activation [57]. Future work should further characterize this range in the cortex by varying amplitude, frequency while decoupling the effects from monophasic cathodic and anodic stimulation.

Electrical stimulation can result in undesired synchronous activity that can result in displeasing sensations and paresthesia at the onset of stimulation [30, 113]. These effects are more common at high frequencies and are thought to be due to large initial synchronous firing followed by habituation or failed entrainment [30, 41]. Our previous study demonstrated that at the onset of stimulation, there is a distributed pattern of neuronal activation followed by inactivation of more distal neurons. They classified the neuronal responses into steady state and onset cells, that were active for the first two and last two seconds of stimulation, or only the first two seconds and not the last two seconds, respectively[41]. Consistent with those results we found a low proportion of onset cells, with a high proportion of steady state cells[41]. We also characterized a rare third class of activation where cells were not active at the onset of stimulation, but became activated by the end of the stimulation train. We defined these as delayed response cells. These cells were more common for cathodic asymmetric stimulation and suggest that, over time, the entrainment probability of neurons increases for these waveforms. It is possible that this increased entrainment over time could be used to encode an increasing perceptual intensity in neural prosthetics. Furthermore, by using pulse waveform asymmetry to modulate the activation of the network of neurons and their processes, it may be possible to increase our ability to encode more complex sensations like texture. Future studies should investigate the perceptual quality of these stimulation waveforms with longer duration stimulation trains.

Neuronal entrainment to electrical stimulation depends on the site of activation, the location of the neuronal elements around the electrode, and the stimulation waveform [38, 39, 49]. Neuronal somas close to the electrode were predicted to entrain better to cathodic asymmetric stimulation with a long leading phase, with distal neurons activated by their fibers were predicted to entrain better to anodic asymmetric stimulation with a long leading phase compared to symmetric cathodic stimulation. In fact, cathodic and anodic asymmetric waveforms were predicted to activate non-overlapping neuronal populations and cathodic symmetric stimulation was predicted to activate neurons in each population. Consistent with this, we show that cathodic asymmetric stimulation activates a subpopulation of the same neurons activated by cathodic symmetric stimulation. In contrast to what was predicted by early modeling studies, the neuronal population activated by anodic asymmetric stimulation had nearly 100% overlap with cathodic symmetric stimulation. Although there was overlap in the population of neurons activated, the location of activation on the neuron may not be the same, which could have different entrainment probabilities. With an activation index, we show that the neurons around the electrode entrain with highly comparable probabilities to cathodic symmetric and asymmetric stimulation, with the majority of neurons preferring highly asymmetric anodic stimulation. This shows that the neuronal population activated by these waveforms is highly similar in the space. Alternatively, the entrainment of the neurons activated in common between the different waveforms had significantly lower entrainment to cathodic asymmetric stimulation with a long leading phase. It will be important to consider the entrainment to higher stimulation frequencies and amplitudes, because neurons can entrain better to higher frequency stimulation when the axon initial segment is activated [48].

Despite the similarity in neuronal activation, the potential modulation of other cell types (inhibitory, non-neuronal) should not be ignored. Additionally, while microglia, and astrocytes are generally not considered to be electrically excitable, they are able to express voltage sensitive ion channels that may be modulated by electrical stimulation to change functional state and regulate neuronal activity [114-119]. Additionally, neuronal activity is known to be modulated by both cell types, and modulation of the astrocytic membrane potential has been shown to have substantial consequences on neuronal

activity[85, 120]. Furthermore, electrode implantation results in an immune response in which activated microglia express voltage gated ion channels around the electrode, therefore becoming susceptible to the effects of stimulation[119]. Lastly, in the context of therapeutic application, deep brain stimulation has been effective in treating many disorders, however, the onset effects can be variable[24, 27, 113, 121-124]. Granted the mechanisms responsible for this variation are largely unknown, the role of non-neuronal cells should not be ignored.

4.5 Limitations

This study used *in vivo* calcium imaging to address the hypothesis that stimulation waveform can modulate the spatial distribution and entrainment of neurons around the electrode. The guiding principle behind the use of asymmetric waveforms is that the long duration leading phase can modulate the activation probability of different neuronal elements and lead to either selective orthodromic (cathodic first) or antidromic (anodic first) activation. Due to the kinetics and spatial localization of the calcium sensor used in this study, we are unable to confirm the location of stimulation initiation nor the timing of individual action potentials. Additionally, although we interpret greater spread of activation to be an increased probability of antidromic activation, we cannot separate direct synaptic activation from indirect activation through synaptic transmission. Future experiments should use excitatory synaptic blockers (*e.g.* CNQX, APV) to confirm the role of indirect activation on longer time and spatial scales. Additionally, because the calcium sensor used in this study (GCaMP6s) increases fluorescence with the number of action potential in short succession [58], we defined entrainment here to refer to the ability of neurons or neuropil to result in activation to greater, or lesser percentage of stimulation pulses as measured by a larger increase in fluorescence. Importantly, it is not clear whether the increased fluorescence intensity is a result of greater 1:1 entrainment, or due to other activation properties such and bursting. Newer developments in genetically encoded voltage (GEVI) and calcium indicators (GECI) with faster kinetics may be able to more comprehensively address these questions [125-127]. However, it should be noted that current GEVIs do not provide comparable spatial resolution and suffer from lower signal to noise ratio[128].

Additionally, while highly valuable for spatial resolution, due to the limitations of two-photon imaging, we could only observe direct neuronal activation within the imaging plane. Newer developments in light sheet [129], or even swept confocally-aligned planar excitation (SCAPE) imaging [130] could be suited to observe not only the horizontal activation but also the activation between cortical layers at higher speeds. It is also important to note that this study was conducted in an acute preparation necessitating the use of anesthesia. Here we used ketamine, which is a known NMDA antagonist and $GABA_A$ potentiator, thus modulating the baseline probability of neuronal activation and entrainment [131-133]. Future studies should be conducted in awake preparations, yet, taking care to consider the large influence on neuronal damage, microglial activation, and astroglia scarring, which are suggested to modulate both recording and stimulation[92, 134, 135]. Additionally, there is a need to directly evaluate how stimulation induced activity changes over time in a chronic setting given the dynamic tissue responses to implantable electrodes [125]. These studies could help explain the variability in response to stimulation that has been observed. It is important to note that higher frequency stimulation (*e.g.* 100 Hz) is often used in therapeutic settings, while this study investigated 10 Hz stimulation[11, 24, 27, 121]. We chose 10 Hz stimulation to reduce the onset effect observed at higher frequencies[30, 41], but given the significant results observed here, future studies should investigate how stimulation frequency may also interact with asymmetry and polarity. Lastly, GCaMP6s was expressed predominately in excitatory pyramidal cells, while inhibitory cells play an essential role in the lateral spread of neuronal stimulation. To fully understand the role of stimulation waveform on neuronal activation patterns, it is critical to investigate the effect on inhibitory neurons.

Conclusion

Using calcium imaging, we have demonstrated that stimulation waveform and polarity largely interact in the spatial recruitment of neurons. We specifically demonstrate that as asymmetry index increases in cathodic first pulses, the spatial localization increases and level of neuronal activation decreases. Conversely, in anodic first pulses, the activity level and spatial distribution begins to better resemble conventional symmetric cathodic leading stimulation. We show that even at 10 Hz there is a spatial fall off of neuronal activity to stimulation over a 30s train. Additionally, there is a prolonged period of inactivity following stimulation that scales with the level of activation during stimulation. Importantly, this demonstrates the potential for stimulation waveform in modulating neuronal activity for different therapeutic applications, or even elicitation of complex sensory percepts. Furthermore, with the widespread use of electrical stimulation in circuit analysis, we provide evidence of stimulation parameters that can increase spatial selectivity and limit the activation of passing fibers from different circuits. Thus, stimulation polarity and asymmetry can therefore be used to investigate the role of neuronal entrainment and activity within a target circuit.

Acknowledgments
This work was supported by NIH R01NS094396, R01NS105691, and R21NS108098 and the ARCS Foundation, Inc., Pittsburgh Chapter, Gookin Family Foundation Award.

Conflict of Interest
The authors declare no competing interests.

Author Contributions
Conceptualization, All authors; *Methodology*, All authors; *Investigation,* K.C.S., *Formal Analysis*, K.C.S. and J.R.E. *Writing—Original Draft*, T.D.Y.K., and K.C.S.; *Writing—Review & Editing*, All authors; *Visualization*, K.C.S and T.D.Y.K.; *Supervision*, T.D.Y.K.; *Funding Acquisition*, T.D.Y.K.

Bibliography
[1] C.D. Salzman, K.H. Britten, W.T. Newsome, Cortical microstimulation influences perceptual judgements of motion direction, Nature 346(6280) (1990) 174-7.
[2] E.J. Tehovnik, W.M. Slocum, Microstimulation of macaque V1 disrupts target selection: effects of stimulation polarity, Experimental brain research 148(2) (2003) 233-7.
[3] E.J. Tehovnik, W.M. Slocum, P.H. Schiller, Saccadic eye movements evoked by microstimulation of striate cortex, The European journal of neuroscience 17(4) (2003) 870-8.
[4] M. Armenta Salas, L. Bashford, S. Kellis, M. Jafari, H. Jo, D. Kramer, K. Shanfield, K. Pejsa, B. Lee, C.Y. Liu, R.A. Andersen, Proprioceptive and cutaneous sensations in humans elicited by intracortical microstimulation, Elife 7 (2018).
[5] J.A. Berg, J.F. Dammann, 3rd, F.V. Tenore, G.A. Tabot, J.L. Boback, L.R. Manfredi, M.L. Peterson, K.D. Katyal, M.S. Johannes, A. Makhlin, R. Wilcox, R.K. Franklin, R.J. Vogelstein, N.G. Hatsopoulos, S.J. Bensmaia, Behavioral demonstration of a somatosensory neuroprosthesis, IEEE Trans Neural Syst Rehabil Eng 21(3) (2013) 500-7.
[6] W.H. Bosking, M.S. Beauchamp, D. Yoshor, Electrical Stimulation of Visual Cortex: Relevance for the Development of Visual Cortical Prosthetics, Annual Review of Vision Science 3(1) (2017) 141-166.
[7] D.C. Bradley, P.R. Troyk, J.A. Berg, M. Bak, S. Cogan, R. Erickson, C. Kufta, M. Mascaro, D. McCreery, E.M. Schmidt, V.L. Towle, H. Xu, Visuotopic mapping through a multichannel stimulating implant in primate V1, Journal of neurophysiology 93(3) (2005) 1659-70.
[8] S. Butovas, C. Schwarz, Spatiotemporal effects of microstimulation in rat neocortex: a parametric study using multielectrode recordings, Journal of neurophysiology 90(5) (2003) 3024-39.
[9] S. Butovas, C. Schwarz, Detection psychophysics of intracortical microstimulation in rat primary somatosensory cortex, The European journal of neuroscience 25(7) (2007) 2161-9.

[10] N. Cicmil, K. Krug, Playing the electric light orchestra—how electrical stimulation of visual cortex elucidates the neural basis of perception, Philosophical Transactions of the Royal Society B: Biological Sciences 370(1677) (2015).
[11] S.N. Flesher, J.L. Collinger, S.T. Foldes, J.M. Weiss, J.E. Downey, E.C. Tyler-Kabara, S.J. Bensmaia, A.B. Schwartz, M.L. Boninger, R.A. Gaunt, Intracortical microstimulation of human somatosensory cortex, Sci Transl Med 8(361) (2016) 361ra141.
[12] G.Y. Fridman, H.T. Blair, A.P. Blaisdell, J.W. Judy, Perceived intensity of somatosensory cortical electrical stimulation, Experimental brain research 203(3) (2010) 499-515.
[13] W.M. Grill, Frontiers in Neuroengineering
Signal Considerations for Chronically Implanted Electrodes for Brain Interfacing, in: W.M. Reichert (Ed.), Indwelling Neural Implants: Strategies for Contending with the In Vivo Environment, CRC Press/Taylor & Francis
Taylor & Francis Group, LLC., Boca Raton (FL), 2008.
[14] W.M. Grill, S.E. Norman, R.V. Bellamkonda, Implanted neural interfaces: biochallenges and engineered solutions, Annual review of biomedical engineering 11 (2009) 1-24.
[15] C.W. Hess, D.E. Vaillancourt, M.S. Okun, The temporal pattern of stimulation may be important to the mechanism of deep brain stimulation, Experimental neurology 247 (2013) 296-302.
[16] S. Kim, T. Callier, S.J. Bensmaia, A computational model that predicts behavioral sensitivity to intracortical microstimulation, J Neural Eng 14(1) (2017) 016012.
[17] S. Kim, T. Callier, G.A. Tabot, R.A. Gaunt, F.V. Tenore, S.J. Bensmaia, Behavioral assessment of sensitivity to intracortical microstimulation of primate somatosensory cortex, Proc Natl Acad Sci U S A 112(49) (2015) 15202-7.
[18] R. Romo, A. Hernandez, A. Zainos, C.D. Brody, L. Lemus, Sensing without touching: psychophysical performance based on cortical microstimulation, Neuron 26(1) (2000) 273-8.
[19] R. Romo, A. Hernandez, A. Zainos, E. Salinas, Somatosensory discrimination based on cortical microstimulation, Nature 392(6674) (1998) 387-90.
[20] H.P. Saal, S.J. Bensmaia, Biomimetic approaches to bionic touch through a peripheral nerve interface, Neuropsychologia 79(Pt B) (2015) 344-53.
[21] P.H. Schiller, W.M. Slocum, M.C. Kwak, G.L. Kendall, E.J. Tehovnik, New methods devised specify the size and color of the spots monkeys see when striate cortex (area V1) is electrically stimulated, Proc Natl Acad Sci U S A 108(43) (2011) 17809-14.
[22] E.M. Schmidt, M.J. Bak, F.T. Hambrecht, C.V. Kufta, D.K. O'Rourke, P. Vallabhanath, Feasibility of a visual prosthesis for the blind based on intracortical microstimulation of the visual cortex, Brain : a journal of neurology 119 (Pt 2) (1996) 507-22.
[23] E.J. Tehovnik, W.M. Slocum, Two-photon imaging and the activation of cortical neurons, Neuroscience 245 (2013) 12-25.
[24] D.L. Byrd, W.J. Marks, Jr., P.A. Starr, Deep brain stimulation for advanced Parkinson's disease, AORN journal 72(3) (2000) 387-90, 393-408; quiz 409-14, 416-8.
[25] R. Fisher, V. Salanova, T. Witt, R. Worth, T. Henry, R. Gross, K. Oommen, I. Osorio, J. Nazzaro, D. Labar, M. Kaplitt, M. Sperling, E. Sandok, J. Neal, A. Handforth, J. Stern, A. DeSalles, S. Chung, A. Shetter, D. Bergen, R. Bakay, J. Henderson, J. French, G. Baltuch, W. Rosenfeld, A. Youkilis, W. Marks, P. Garcia, N. Barbaro, N. Fountain, C. Bazil, R. Goodman, G. McKhann, K. Babu Krishnamurthy, S. Papavassiliou, C. Epstein, J. Pollard, L. Tonder, J. Grebin, R. Coffey, N. Graves, Electrical stimulation of the anterior nucleus of thalamus for treatment of refractory epilepsy, Epilepsia 51(5) (2010) 899-908.
[26] L. Garcia-Larrea, R. Peyron, P. Mertens, M.C. Gregoire, F. Lavenne, D. Le Bars, P. Convers, F. Mauguiere, M. Sindou, B. Laurent, Electrical stimulation of motor cortex for pain control: a combined PET-scan and electrophysiological study, Pain 83(2) (1999) 259-73.
[27] T.M. Herrington, J.J. Cheng, E.N. Eskandar, Mechanisms of deep brain stimulation, Journal of neurophysiology 115(1) (2016) 19-38.
[28] J.D. Lieber, S.J. Bensmaia, High-dimensional representation of texture in somatosensory cortex of primates, Proc Natl Acad Sci U S A 116(8) (2019) 3268-3277.

[29] D.N. Anderson, G. Duffley, J. Vorwerk, A.C. Dorval, C.R. Butson, Anodic Stimulation Misunderstood: Preferential Activation of Fiber Orientations with Anodic Waveforms in Deep Brain Stimulation, J Neural Eng (2018).
[30] Z. Cai, Z. Feng, Z. Guo, W. Zhou, Z. Wang, X. Wei, Novel Stimulation Paradigms with Temporally-Varying Parameters to Reduce Synchronous Activity at the Onset of High Frequency Stimulation in Rat Hippocampus, Frontiers in neuroscience 11 (2017) 563.
[31] B.P. Delhaye, H.P. Saal, S.J. Bensmaia, Key considerations in designing a somatosensory neuroprosthesis, Journal of physiology, Paris 110(4 Pt A) (2016) 402-408.
[32] W.M. Grill, Temporal Pattern of Electrical Stimulation is a New Dimension of Therapeutic Innovation, Current opinion in biomedical engineering 8 (2018) 1-6.
[33] M.H. Histed, V. Bonin, R.C. Reid, Direct activation of sparse, distributed populations of cortical neurons by electrical microstimulation, Neuron 63(4) (2009) 508-22.
[34] L. Hofmann, M. Ebert, P.A. Tass, C. Hauptmann, Modified pulse shapes for effective neural stimulation, Frontiers in neuroengineering 4 (2011) 9.
[35] A.S. Koivuniemi, K.J. Otto, Asymmetric versus symmetric pulses for cortical microstimulation, IEEE Trans Neural Syst Rehabil Eng 19(5) (2011) 468-76.
[36] A.M. Kuncel, W.M. Grill, Selection of stimulus parameters for deep brain stimulation, Clinical neurophysiology : official journal of the International Federation of Clinical Neurophysiology 115(11) (2004) 2431-41.
[37] O. Macherey, A. van Wieringen, R.P. Carlyon, J.M. Deeks, J. Wouters, Asymmetric pulses in cochlear implants: effects of pulse shape, polarity, and rate, J Assoc Res Otolaryngol 7(3) (2006) 253-66.
[38] C.C. McIntyre, W.M. Grill, Selective microstimulation of central nervous system neurons, Ann Biomed Eng 28(3) (2000) 219-33.
[39] C.C. McIntyre, W.M. Grill, Extracellular stimulation of central neurons: influence of stimulus waveform and frequency on neuronal output, Journal of neurophysiology 88(4) (2002) 1592-604.
[40] C.C. McIntyre, A.G. Richardson, W.M. Grill, Modeling the excitability of mammalian nerve fibers: influence of afterpotentials on the recovery cycle, Journal of neurophysiology 87(2) (2002) 995-1006.
[41] N.J. Michelson, J.R. Eles, A.L. Vazquez, K.A. Ludwig, T.D.Y. Kozai, Calcium activation of cortical neurons by continuous electrical stimulation: Frequency dependence, temporal fidelity, and activation density, Journal of neuroscience research 97(5) (2019) 620-638.
[42] B. Wark, B.N. Lundstrom, A. Fairhall, Sensory adaptation, Current opinion in neurobiology 17(4) (2007) 423-9.
[43] A. Branner, R.B. Stein, E. Fernandez, Y. Aoyagi, R.A. Normann, Long-term stimulation and recording with a penetrating microelectrode array in cat sciatic nerve, IEEE Trans Biomed Eng 51(1) (2004) 146-57.
[44] J.B. Ranck, Jr., Which elements are excited in electrical stimulation of mammalian central nervous system: a review, Brain Res 98(3) (1975) 417-40.
[45] L.G. Nowak, J. Bullier, Axons, but not cell bodies, are activated by electrical stimulation in cortical gray matter. I. Evidence from chronaxie measurements, Experimental brain research 118(4) (1998) 477-88.
[46] L.G. Nowak, J. Bullier, Axons, but not cell bodies, are activated by electrical stimulation in cortical gray matter. II. Evidence from selective inactivation of cell bodies and axon initial segments, Experimental brain research 118(4) (1998) 489-500.
[47] A.S. Aberra, A.V. Peterchev, W.M. Grill, Biophysically realistic neuron models for simulation of cortical stimulation, J Neural Eng 15(6) (2018) 066023.
[48] M. Radivojevic, D. Jackel, M. Altermatt, J. Muller, V. Viswam, A. Hierlemann, D.J. Bakkum, Electrical Identification and Selective Microstimulation of Neuronal Compartments Based on Features of Extracellular Action Potentials, Sci Rep 6 (2016) 31332.
[49] G. Yi, W.M. Grill, Frequency-dependent antidromic activation in thalamocortical relay neurons: effects of synaptic inputs, J Neural Eng 15(5) (2018) 056001.

[50] R.J. Greenberg, T.J. Velte, M.S. Humayun, G.N. Scarlatis, E. de Juan, Jr., A computational model of electrical stimulation of the retinal ganglion cell, IEEE Trans Biomed Eng 46(5) (1999) 505-14.
[51] C.C. McIntyre, W.M. Grill, Excitation of central nervous system neurons by nonuniform electric fields, Biophysical journal 76(2) (1999) 878-88.
[52] F. Rattay, Analysis of models for external stimulation of axons, IEEE Trans Biomed Eng 33(10) (1986) 974-7.
[53] B. Gustafsson, E. Jankowska, Direct and indirect activation of nerve cells by electrical pulses applied extracellularly, The Journal of physiology 258(1) (1976) 33-61.
[54] D.R. Merrill, M. Bikson, J.G. Jefferys, Electrical stimulation of excitable tissue: design of efficacious and safe protocols, J Neurosci Methods 141(2) (2005) 171-98.
[55] S.F. Cogan, Neural stimulation and recording electrodes, Annual review of biomedical engineering 10 (2008) 275-309.
[56] D. Kumsa, E.M. Hudak, F.W. Montague, S.C. Kelley, D.F. Untereker, B.P. Hahn, C. Condit, M. Cholette, H. Lee, D. Bardot, P. Takmakov, Electrical neurostimulation with imbalanced waveform mitigates dissolution of platinum electrodes, J Neural Eng 13(5) (2016) 054001.
[57] Q. Wang, D.C. Millard, H.J. Zheng, G.B. Stanley, Voltage-sensitive dye imaging reveals improved topographic activation of cortex in response to manipulation of thalamic microstimulation parameters, J Neural Eng 9(2) (2012) 026008.
[58] T.W. Chen, T.J. Wardill, Y. Sun, S.R. Pulver, S.L. Renninger, A. Baohan, E.R. Schreiter, R.A. Kerr, M.B. Orger, V. Jayaraman, L.L. Looger, K. Svoboda, D.S. Kim, Ultrasensitive fluorescent proteins for imaging neuronal activity, Nature 499(7458) (2013) 295-300.
[59] J.R. Eles, A.L. Vazquez, T.D.Y. Kozai, X.T. Cui, In vivo imaging of neuronal calcium during electrode implantation: Spatial and temporal mapping of damage and recovery, Biomaterials 174 (2018) 79-94.
[60] J.R. Eles, A.L. Vazquez, N.R. Snyder, C. Lagenaur, M.C. Murphy, T.D. Kozai, X.T. Cui, Neuroadhesive L1 coating attenuates acute microglial attachment to neural electrodes as revealed by live two-photon microscopy, Biomaterials 113 (2017) 279-292.
[61] T.D.Y. Kozai, A.S. Jaquins-Gerstl, A.L. Vazquez, A.C. Michael, X.T. Cui, Dexamethasone retrodialysis attenuates microglial response to implanted probes in vivo, Biomaterials 87 (2016) 157-169.
[62] T.D. Kozai, A.L. Vazquez, C.L. Weaver, S.G. Kim, X.T. Cui, In vivo two-photon microscopy reveals immediate microglial reaction to implantation of microelectrode through extension of processes, J Neural Eng 9(6) (2012) 066001.
[63] N.J. Michelson, A.L. Vazquez, J.R. Eles, J.W. Salatino, E.K. Purcell, J.J. Williams, X.T. Cui, T.D.Y. Kozai, Multi-scale, multi-modal analysis uncovers complex relationship at the brain tissue-implant neural interface: new emphasis on the biological interface, J Neural Eng 15(3) (2018) 033001.
[64] T.D. Kozai, X. Li, L.M. Bodily, E.M. Caparosa, G.A. Zenonos, D.L. Carlisle, R.M. Friedlander, X.T. Cui, Effects of caspase-1 knockout on chronic neural recording quality and longevity: insight into cellular and molecular mechanisms of the reactive tissue response, Biomaterials 35(36) (2014) 9620-34.
[65] J.R. Eles, A.L. Vazquez, T.D.Y. Kozai, X.T. Cui, Meningeal inflammatory response and fibrous tissue remodeling around intracortical implants: An in vivo two-photon imaging study, Biomaterials 195 (2019) 111-123.
[66] T.D. Kozai, J.R. Eles, A.L. Vazquez, X.T. Cui, Two-photon imaging of chronically implanted neural electrodes: Sealing methods and new insights, J Neurosci Methods 258 (2016) 46-55.
[67] S.M. Wellman, T.D.Y. Kozai, In vivo spatiotemporal dynamics of NG2 glia activity caused by neural electrode implantation, Biomaterials 164 (2018) 121-133.
[68] K.C. Stocking, A.L. Vazquez, T.D.Y. Kozai, Intracortical neural stimulation with untethered, ultrasmall carbon fiber electrodes mediated by the photoelectric effect, Ieee T Bio-Med Eng (2019).

[69] S. Eick, J. Wallys, B. Hofmann, A. van Ooyen, U. Schnakenberg, S. Ingebrandt, A. Offenhäusser, Iridium oxide microelectrode arrays for in vitro stimulation of individual rat neurons from dissociated cultures, Frontiers in neuroengineering 2 (2009) 16.
[70] D. McCreery, V. Pikov, P.R. Troyk, Neuronal loss due to prolonged controlled-current stimulation with chronically implanted microelectrodes in the cat cerebral cortex, J Neural Eng 7(3) (2010) 036005.
[71] R.V. Shannon, A model of safe levels for electrical stimulation, IEEE Trans Biomed Eng 39(4) (1992) 424-6.
[72] D.B. McCreery, W.F. Agnew, L.A. Bullara, The effects of prolonged intracortical microstimulation on the excitability of pyramidal tract neurons in the cat, Ann Biomed Eng 30(1) (2002) 107-19.
[73] D.B. McCreery, W.F. Agnew, T.G. Yuen, L. Bullara, Charge density and charge per phase as cofactors in neural injury induced by electrical stimulation, IEEE Trans Biomed Eng 37(10) (1990) 996-1001.
[74] S.F. Cogan, K.A. Ludwig, C.G. Welle, P. Takmakov, Tissue damage thresholds during therapeutic electrical stimulation, J Neural Eng 13(2) (2016) 021001.
[75] S.F. Cogan, P.R. Troyk, J. Ehrlich, T.D. Plante, D.E. Detlefsen, Potential-biased, asymmetric waveforms for charge-injection with activated iridium oxide (AIROF) neural stimulation electrodes, IEEE Trans Biomed Eng 53(2) (2006) 327-32.
[76] Y. Ma, M.A. Shaik, M.G. Kozberg, S.H. Kim, J.P. Portes, D. Timerman, E.M. Hillman, Resting-state hemodynamics are spatiotemporally coupled to synchronized and symmetric neural activity in excitatory neurons, Proc Natl Acad Sci U S A 113(52) (2016) E8463-e8471.
[77] R. Rehani, Y. Atamna, L. Tiroshi, W.H. Chiu, J. de Jesús Aceves Buendía, G.J. Martins, G.A. Jacobson, J.A. Goldberg, Activity Patterns in the Neuropil of Striatal Cholinergic Interneurons in Freely Moving Mice Represent Their Collective Spiking Dynamics, eNeuro 6(1) (2019).
[78] S. Lee, J.F. Meyer, J. Park, S.M. Smirnakis, Visually Driven Neuropil Activity and Information Encoding in Mouse Primary Visual Cortex, Frontiers in Neural Circuits 11(50) (2017).
[79] A.S. Tolias, F. Sultan, M. Augath, A. Oeltermann, E.J. Tehovnik, P.H. Schiller, N.K. Logothetis, Mapping cortical activity elicited with electrical microstimulation using FMRI in the macaque, Neuron 48(6) (2005) 901-11.
[80] E.J. Tehovnik, A.S. Tolias, F. Sultan, W.M. Slocum, N.K. Logothetis, Direct and indirect activation of cortical neurons by electrical microstimulation, Journal of neurophysiology 96(2) (2006) 512-21.
[81] S.H. Bitzenhofer, J. Ahlbeck, A. Wolff, J.S. Wiegert, C.E. Gee, T.G. Oertner, I.L. Hanganu-Opatz, Layer-specific optogenetic activation of pyramidal neurons causes beta-gamma entrainment of neonatal networks, Nature communications 8 (2017) 14563.
[82] L.D. Pozzo-Miller, W. Gottschalk, L. Zhang, K. McDermott, J. Du, R. Gopalakrishnan, C. Oho, Z.H. Sheng, B. Lu, Impairments in high-frequency transmission, synaptic vesicle docking, and synaptic protein distribution in the hippocampus of BDNF knockout mice, The Journal of neuroscience : the official journal of the Society for Neuroscience 19(12) (1999) 4972-83.
[83] B.A. Bari, D.R. Ollerenshaw, D.C. Millard, Q. Wang, G.B. Stanley, Behavioral and electrophysiological effects of cortical microstimulation parameters, PloS one 8(12) (2013) e82170.
[84] C.C. McIntyre, W.A. Grill, Model-based design of stimulus trains for selective microstimulation of targeted neuronal populations, 2001 Conference Proceedings of the 23rd Annual International Conference of the IEEE Engineering in Medicine and Biology Society, 2001, pp. 806-809 vol.1.
[85] J.A. Gomez, J.M. Perkins, G.M. Beaudoin, N.B. Cook, S.A. Quraishi, E.A. Szoeke, K. Thangamani, C.W. Tschumi, M.J. Wanat, A.M. Maroof, M.J. Beckstead, P.A. Rosenberg, C.A. Paladini, Ventral tegmental area astrocytes orchestrate avoidance and approach behavior, Nature communications 10(1) (2019) 1455.
[86] A.A. Brock, R.M. Friedman, R.H. Fan, A.W. Roe, Optical imaging of cortical networks via intracortical microstimulation, Journal of neurophysiology 110(11) (2013) 2670-8.
[87] M. Osanai, S. Tanaka, Y. Takeno, S. Takimoto, T. Yagi, Spatiotemporal properties of the action potential propagation in the mouse visual cortical slice analyzed by calcium imaging, PloS one 5(10) (2010) e13738.

[88] G.P. Thomas, B.C. Jobst, Critical review of the responsive neurostimulator system for epilepsy, Med Devices (Auckl) 8 (2015) 405-11.
[89] A. Campbell, C. Wu, Chronically Implanted Intracranial Electrodes: Tissue Reaction and Electrical Changes, Micromachines (Basel) 9(9) (2018).
[90] E.V. Platia, J.A. Brinker, Time course of transvenous pacemaker stimulation impedance, capture threshold, and electrogram amplitude, Pacing Clin Electrophysiol 9(5) (1986) 620-5.
[91] A. Gittis, Probing new targets for movement disorders, Science 361(6401) (2018) 462-462.
[92] A.N.A. Kozai T.D.Y., Zhang H., Kotov N.A., Gaunt R.A., Cui X.T., Nanostructured Coatings for Improved Charge Delivery to Neurons, in: M.L. De Vittorio M., Assad J. (Ed.), Nanotechnology and Neuroscience: Nano-electronic, Photonic and Mechanical Neuronal Interfacing, Springer, New York, NY, 2014.
[93] C.C. McIntyre, W.M. Grill, Excitation of Central Nervous System Neurons by Nonuniform Electric Fields, Biophysical Journal 76(2) (1999) 878-888.
[94] S.D. Stoney, Jr., W.D. Thompson, H. Asanuma, Excitation of pyramidal tract cells by intracortical microstimulation: effective extent of stimulating current, Journal of neurophysiology 31(5) (1968) 659-69.
[95] J.a.B. Mortimer, N, Peripheral Nerve and Muscle Stimulation, World Scientific Publishing Co. Pte. Ltd., Singapore, 2004.
[96] A.J. Fenoy, L. Goetz, S. Chabardes, Y. Xia, Deep brain stimulation: are astrocytes a key driver behind the scene?, CNS neuroscience & therapeutics 20(3) (2014) 191-201.
[97] J.P. Gottlieb, A. Keller, Intrinsic circuitry and physiological properties of pyramidal neurons in rat barrel cortex, Experimental brain research 115(1) (1997) 47-60.
[98] D. Debanne, Information processing in the axon, Nature Reviews Neuroscience 5(4) (2004) 304-316.
[99] J.P. Meeks, S. Mennerick, Selective effects of potassium elevations on glutamate signaling and action potential conduction in hippocampus, The Journal of neuroscience : the official journal of the Society for Neuroscience 24(1) (2004) 197-206.
[100] D.B. McCreery, W.F. Agnew, Changes in extracellular potassium and calcium concentration and neural activity during prolonged electrical stimulation of the cat cerebral cortex at defined charge densities, Experimental neurology 79(2) (1983) 371-96.
[101] H A Swadlow, a. J D Kocsis, S.G. Waxman, Modulation of Impulse Conduction Along the Axonal Tree, Annual review of biophysics and bioengineering 9(1) (1980) 143-179.
[102] J.C. Octeau, M.R. Gangwani, S.L. Allam, D. Tran, S. Huang, T.M. Hoang-Trong, P. Golshani, T.H. Rumbell, J.R. Kozloski, B.S. Khakh, Transient, Consequential Increases in Extracellular Potassium Ions Accompany Channelrhodopsin2 Excitation, Cell reports 27(8) (2019) 2249-2261.e7.
[103] Y. Tanaka, T. Nomoto, T. Shiki, Y. Sakata, Y. Shimada, Y. Hayashida, T. Yagi, Focal activation of neuronal circuits induced by microstimulation in the visual cortex, J Neural Eng 16(3) (2019) 036007.
[104] A.T. Hussin, J.A. Boychuk, A.R. Brown, Q.J. Pittman, G.C. Teskey, Intracortical Microstimulation (ICMS) Activates Motor Cortex Layer 5 Pyramidal Neurons Mainly Transsynaptically, Brain stimulation 8(4) (2015) 742-50.
[105] X. Yu, A.M.W. Taylor, J. Nagai, P. Golshani, C.J. Evans, G. Coppola, B.S. Khakh, Reducing Astrocyte Calcium Signaling In Vivo Alters Striatal Microcircuits and Causes Repetitive Behavior, Neuron 99(6) (2018) 1170-1187.e9.
[106] B.S. Khakh, Astrocyte-Neuron Interactions in the Striatum: Insights on Identity, Form, and Function, Trends in neurosciences 42(9) (2019) 617-630.
[107] J.S. Marvin, Y. Shimoda, V. Magloire, M. Leite, T. Kawashima, T.P. Jensen, I. Kolb, E.L. Knott, O. Novak, K. Podgorski, N.J. Leidenheimer, D.A. Rusakov, M.B. Ahrens, D.M. Kullmann, L.L. Looger, A genetically encoded fluorescent sensor for in vivo imaging of GABA, Nature Methods 16(8) (2019) 763-770.
[108] D.T. Brocker, B.D. Swan, R.Q. So, D.A. Turner, R.E. Gross, W.M. Grill, Optimized temporal pattern of brain stimulation designed by computational evolution, Sci Transl Med 9(371) (2017).

[109] N. Palomero-Gallagher, K. Zilles, Cortical layers: Cyto-, myelo-, receptor- and synaptic architecture in human cortical areas, NeuroImage 197 (2019) 716-741.
[110] S. Geyer, A. Schleicher, K. Zilles, The Somatosensory Cortex of Human: Cytoarchitecture and Regional Distributions of Receptor-Binding Sites, NeuroImage 6(1) (1997) 27-45.
[111] P.A. House, J.D. MacDonald, P.A. Tresco, R.A. Normann, Acute microelectrode array implantation into human neocortex: preliminary technique and histological considerations, Neurosurgical focus 20(5) (2006) E4.
[112] M. Paulussen, S. Jacobs, E. Van der Gucht, P.R. Hof, L. Arckens, Cytoarchitecture of the mouse neocortex revealed by the low-molecular-weight neurofilament protein subunit, Brain Struct Funct 216(3) (2011) 183-99.
[113] A.M. Kuncel, S.E. Cooper, B.R. Wolgamuth, M.A. Clyde, S.A. Snyder, E.B. Montgomery, Jr., A.R. Rezai, W.M. Grill, Clinical response to varying the stimulus parameters in deep brain stimulation for essential tremor, Movement disorders : official journal of the Movement Disorder Society 21(11) (2006) 1920-8.
[114] H. Sontheimer, Voltage-dependent ion channels in glial cells, Glia 11(2) (1994) 156-72.
[115] A.K. Gellner, J. Reis, B. Fritsch, Glia: A Neglected Player in Non-invasive Direct Current Brain Stimulation, Front Cell Neurosci 10 (2016) 188.
[116] W. Tang, K. Szokol, V. Jensen, R. Enger, C.A. Trivedi, Ø. Hvalby, P.J. Helm, L.L. Looger, R. Sprengel, E.A. Nagelhus, Stimulation-Evoked Ca²⁺ Signals in Astrocytic Processes at Hippocampal CA3–CA1 Synapses of Adult Mice Are Modulated by Glutamate and ATP, The Journal of Neuroscience 35(7) (2015) 3016.
[117] L. Bekar, W. Libionka, G.-F. Tian, Q. Xu, A. Torres, X. Wang, D. Lovatt, E. Williams, T. Takano, J. Schnermann, R. Bakos, M. Nedergaard, Adenosine is crucial for deep brain stimulation–mediated attenuation of tremor, Nature medicine 14 (2007) 75.
[118] N.J. Allen, D.A. Lyons, Glia as architects of central nervous system formation and function, Science 362(6411) (2018) 181-185.
[119] M.J. Stebbing, J.M. Cottee, I. Rana, The Role of Ion Channels in Microglial Activation and Proliferation - A Complex Interplay between Ligand-Gated Ion Channels, K(+) Channels, and Intracellular Ca(2.), Front Immunol 6 (2015) 497.
[120] E.M. York, L.P. Bernier, B.A. MacVicar, Microglial modulation of neuronal activity in the healthy brain, Dev Neurobiol 78(6) (2018) 593-603.
[121] H.S. Mayberg, A.M. Lozano, V. Voon, H.E. McNeely, D. Seminowicz, C. Hamani, J.M. Schwalb, S.H. Kennedy, Deep Brain Stimulation for Treatment-Resistant Depression, Neuron 45(5) (2005) 651-660.
[122] F. Agnesi, M.D. Johnson, J.L. Vitek, Deep brain stimulation: how does it work?, Handb Clin Neurol 116 (2013) 39-54.
[123] B.D. Greenberg, L.A. Gabriels, D.A. Malone, Jr., A.R. Rezai, G.M. Friehs, M.S. Okun, N.A. Shapira, K.D. Foote, P.R. Cosyns, C.S. Kubu, P.F. Malloy, S.P. Salloway, J.E. Giftakis, M.T. Rise, A.G. Machado, K.B. Baker, P.H. Stypulkowski, W.K. Goodman, S.A. Rasmussen, B.J. Nuttin, Deep brain stimulation of the ventral internal capsule/ventral striatum for obsessive-compulsive disorder: worldwide experience, Molecular psychiatry 15(1) (2010) 64-79.
[124] P. Temperli, J. Ghika, J.G. Villemure, P.R. Burkhard, J. Bogousslavsky, F.J. Vingerhoets, How do parkinsonian signs return after discontinuation of subthalamic DBS?, Neurology 60(1) (2003) 78-81.
[125] T. Patriarchi, J.R. Cho, K. Merten, M.W. Howe, A. Marley, W.H. Xiong, R.W. Folk, G.J. Broussard, R. Liang, M.J. Jang, H. Zhong, D. Dombeck, M. von Zastrow, A. Nimmerjahn, V. Gradinaru, J.T. Williams, L. Tian, Ultrafast neuronal imaging of dopamine dynamics with designed genetically encoded sensors, Science 360(6396) (2018).
[126] N. Helassa, B. Podor, A. Fine, K. Torok, Design and mechanistic insight into ultrafast calcium indicators for monitoring intracellular calcium dynamics, Sci Rep 6 (2016) 38276.
[127] Y. Bando, M. Sakamoto, S. Kim, I. Ayzenshtat, R. Yuste, Comparative Evaluation of Genetically Encoded Voltage Indicators, Cell reports 26(3) (2019) 802-813.e4.

[128] K.D. Piatkevich, S. Bensussen, H.-a. Tseng, S.N. Shroff, V.G. Lopez-Huerta, D. Park, E.E. Jung, O.A. Shemesh, C. Straub, H.J. Gritton, M.F. Romano, E. Costa, B.L. Sabatini, Z. Fu, E.S. Boyden, X. Han, Population imaging of neural activity in awake behaving mice in multiple brain regions, bioRxiv (2019) 616094.
[129] S. Wolf, W. Supatto, G. Debrégeas, P. Mahou, S.G. Kruglik, J.-M. Sintes, E. Beaurepaire, R. Candelier, Whole-brain functional imaging with two-photon light-sheet microscopy, Nature Methods 12 (2015) 379.
[130] M.B. Bouchard, V. Voleti, C.S. Mendes, C. Lacefield, W.B. Grueber, R.S. Mann, R.M. Bruno, E.M.C. Hillman, Swept confocally-aligned planar excitation (SCAPE) microscopy for high-speed volumetric imaging of behaving organisms, Nature Photonics 9 (2015) 113.
[131] A. McGirr, J. LeDue, A.W. Chan, Y. Xie, T.H. Murphy, Cortical functional hyperconnectivity in a mouse model of depression and selective network effects of ketamine, Brain : a journal of neurology 140(8) (2017) 2210-2225.
[132] N.J. Michelson, T.D.Y. Kozai, Isoflurane and ketamine differentially influence spontaneous and evoked laminar electrophysiology in mouse V1, Journal of neurophysiology 120(5) (2018) 2232-2245.
[133] M.T. Alkire, A.G. Hudetz, G. Tononi, Consciousness and Anesthesia, Science 322(5903) (2008) 876-880.
[134] S.M. Wellman, L. Li, Y. Yaxiaer, I. McNamara, T.D.Y. Kozai, Revealing Spatial and Temporal Patterns of Cell Death, Glial Proliferation, and Blood-Brain Barrier Dysfunction Around Implanted Intracortical Neural Interfaces, Frontiers in neuroscience 13(493) (2019).
[135] N.A. Alba, Z.J. Du, K.A. Catt, T.D. Kozai, X.T. Cui, In Vivo Electrochemical Analysis of a PEDOT/MWCNT Neural Electrode Coating, Biosensors (Basel) 5(4) (2015) 618-46.